Biomedicine & Pharmacotherapy 181 (2024) 117634

Contents lists available at ScienceDirect

Biomedicine & Pharmacotherapy

journal homepage: www.elsevier.com/locate/biopha

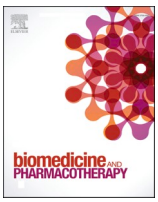

The cell cycle inhibitor p21^{CIP1} is essential for irinotecan-induced senescence and plays a decisive role in re-sensitization of temozolomide-resistant glioblastoma cells to irinotecan

Jason Sallbach , Melanie Woods , Birgit Rasenberger , Markus Christmann [*,1], Maja T. Tomicic [*,2]

Department of Toxicology, University Medical Center of the Johannes Gutenberg University, Obere Zahlbacher Str. 67, Mainz D-55131, Germany

ARTICLE INFO

Keywords:
Glioblastoma
Senescence
Irinotecan
TOP1 inhibitor
P21^{CIP1}
PTEN

ABSTRACT

Background and purpose: Standard of care for glioblastomas includes radio-chemotherapy with the mono-alkylating compound temozolomide. Temozolomide induces primarily senescence, inefficiently killing glioblastoma cells. Recurrences are inevitable. Although recurrences presumably arise from cells evading/escaping TMZ-induced senescence, becoming resistant, they are often again treated with TMZ. As an alternative treatment, irinotecan could be used. Our aim was to examine to what extent and conditions the topoisomerase I inhibitor irinotecan induces senescence and to analyze the underlying mechanism.

Results: Multiple glioblastoma lines with different genetic signatures for p53, p21^{CIP1}, p16^{INK4A}, p14^{ARF}, and PTEN were used. By means of LN229 glioblastoma clones which escaped from temozolomide-induced senescence, thus, being potentially recurrence-forming, we show that this escape is accompanied by increased p21^{CIP1} protein levels in temozolomide-unexposed senescence-evading clones and inability of temozolomide to induce p21^{CIP1}. In contrast, irinotecan was still able to induce p21^{CIP1} and could elevate senescence and cell death. In combination with the senolytic drug BV6, irinotecan-induced senescence was significantly reduced. Differential response clusters were also observed in paired samples of newly diagnosed and recurrent patients' tumors. This can partially explain a significantly prolonged progression-free time until surgery for recurrence in patients additionally treated with irinotecan after temozolomide consolidation and upon the first onset of recurrence.

Conclusions: p21^{CIP1} is essentially involved in induction and maintenance of irinotecan-induced senescence. Neither p16^{INK4A}, p14^{ARF}, nor PTEN contribute to senescence, if p21^{CIP1} cannot be induced. Based on the positive results of the irinotecan/BV6 treatment, combatting recurrent glioblastomas by targeting senescence cell anti-apoptotic pathways (SCAPs) should be considered.

1. Introduction

In 2021 the new WHO classification of central nervous system (CNS) tumors has been published [1]. It relies on additional molecular markers that enable more accuracy and refinement in defining different classes of CNS tumors including glioblastomas (GB). Particularly concerning GB, this might have a huge clinical impact, leading to re-classification of histologically lower astrocytomas into GB, based on those specific molecular markers. Thus, newly diagnosed (former designated as primary) GB correspond to the new classified 'GBM, *IDH*-wildtype' (CNS WHO grade 4) tumor entity with several other mandatory molecular markers (for detailed review, see [2]). *Glioblastoma multiforme* (GBM) is a highly heterogenous and incurable tumor, characterized by diffuse infiltration, aggressiveness, and formation of recurrences. Patients exhibit a dismal prognosis of 14.6 months median survival and a 2-year survival rate of less than 26.5 % [3]. Current treatment comprises surgery (maximum safe resection), radiotherapy, and concomitant and adjuvant chemotherapy with the methylating agent temozolomide (TMZ) [4].

TMZ-induced cytotoxicity (apoptosis) is only achieved in the absence of the alkyl transferase O^6Methylguanine-DNA-methyltransferase (MGMT), thus enabling fixation of O^6Methylguanine (O^6MeG) in the DNA. Subsequently, *via* the functional mismatch repair (MMR),

* Corresponding authors.
E-mail addresses: sallbacj@uni-mainz.de (J. Sallbach), medzulko@uni-mainz.de (M. Woods), rasebi00@uni-mainz.de (B. Rasenberger), mchristm@uni-mainz.de (M. Christmann), tomicic@uni-mainz.de (M.T. Tomicic).
[1] ORCID: 0000–0002-9672–231X
[2] ORCID: 0000–0001-9289–416

https://doi.org/10.1016/j.biopha.2024.117634
Received 14 August 2024; Received in revised form 24 October 2024; Accepted 28 October 2024
Available online 2 November 2024

inserting thymine opposite to O^6MeG (futile MMR cycles), the lesion is converted into DNA double-strand breaks [5–7]. Even under these circumstances, apoptosis is only marginally induced. Instead, TMZ strongly induces senescence in GB cells [8,9]. Cellular senescence pathways in gliomas have been recently reviewed [10]. Some 60 years ago, Hayflick described cellular senescence as a permanent or stable cell cycle arrest that limits the life span of cultured human fibroblasts [11]. Opposite to quiescence (temporary cell cycle arrest), senescence cannot be reverted by proliferative signals [12]. Notably, at the same time, senescent cells can activate tumor-promoting and tumor-suppressing factors, *via* the phenomenon called senescence-associated secretory phenotype (SASP) [13]. SASP is characterized by secretion of interleukins, chemokines, growth factors and matrix metalloproteinases which increase reactive oxygen species (ROS) production and the constant DNA damage response, thus reinforcing the growth arrest [14–17]. Enhancing the therapeutical response, the SASP induces an inflammatory response and activates immune cells which eliminate senescent tumor cells [18,19]. Unfortunately, SASP factors can also enhance malignant tumorigenesis, promote epithelial-mesenchymal transition (EMT) and tumor growth *in vivo* [20–23].

Approx. 90 % of GB patients develop recurrence after the standard therapy (Stupp protocol). There is, however, no established standard of care for recurrent GB, and there is a plethora of therapy options, which are all not curative [24]. One of the often used second-line therapies is the combination of the angiogenic drug Bevacizumab and a topoisomerase I (TOP1) inhibitor irinotecan (IT), which has been administered over a decade in clinical trials or in-house protocols for the treatment of recurrent GB, since IT passes the blood-brain barrier. Just recently, a paper was re-published describing the original clinical trial from 2009 [25]. As in the paper of 2009 concluded, Bevacizumab plus IT was well tolerated and active in recurrent GB. Also, in 2023, *ESMO Open* published retrospective study data on in-house primary GB patients who second-line received Bevacizumab plus IT, in which the authors concluded that this regimen shows activity in recurrent GB and that toxicity (fatigue, diarrhea, anemia and thrombocytopenia) is considered acceptable [26].

The camptothecin derivative IT gets metabolized by cellular carboxylesterases into the active compound SN-38 [27]. This metabolite blocks the TOP1-cleavage complex and so the re-ligation function of TOP1. This event leads to induction of multiple DNA single-strand breaks and in course of replication leads to DNA double-strand breaks and replication stalling/abortive replication [28]. Thus, the action of camptothecin derivatives, and so of IT as well, depends on the active S-phase of replicating tumor cells. This triggers the constant DNA damage response (ATR/ATM – CHK1/CHK2 signaling). At significantly higher concentrations, also transcription can be stalled. In p53-proficient GB cells, TOP1 inhibition induces the S-phase arrest, but particularly a strong CDK/CDC25c-dependent G2/M-phase arrest [27]. Under reduced DNA repair capacity, the arrest becomes stable, enforcing later-on senescence; only a small portion of cells is apoptotic [29].

Transcriptional activation of *CDKN1A* encoding $p21^{CIP1}$ was shown to be a main cause of senescence induction. $p21^{CIP1}$ inhibits various cyclin-dependent kinases (CDKs) and thus arrests the cell cycle [30,31]. Besides $p21^{CIP1}$, two additional factors seem to be important for senescence induction and its maintenance - $p14^{ARF}$ and $p16^{INK4A}$ [32,33]. Both factors are transcribed from the *CDKN2A* gene. Whereas $p16^{INK4A}$ inhibits CDK4 and CDK6 [34], $p14^{ARF}$ stabilizes p53 by sequestering mouse double minute 2 homolog (MDM2), a protein responsible for the degradation of p53 [35–37].

We could show that TMZ-induced senescence in GB cells as well as its maintenance decisively depends on the transcriptional upregulation of *CDKN1A* and expression of the p21 protein, but does not require $p14^{ARF}$/$p16^{INK4A}$ activity [8]. Since the TOP1 inhibitor IT, a prodrug derivative belonging to camptothecins [38], is a relevant drug in therapy of GB recurrences [25], here we investigated to which extent IT can induce senescence in GB cells, and whether induction of $p21^{CIP1}$ is indispensable for this process. By modulating expression of prominent factors, involved in genotoxic stress-induced senescence, such as the cell cycle inhibitors $p21^{CIP1}$, $p14^{ARF}$, $p16^{INK4A}$ and the tumor suppressor PTEN (phosphatase and tensin homolog), the major negative regulator of the PI3K/AKT pathway, we examined how overexpression or knockdown of these players impacts IT-induced senescence in GB cells. We compared six different IT-exposed GB cell lines with different gene signatures in respect to the end points colony formation, cell death, cell cycle progression and senescence. We also examined the response of TMZ-treated senescence-escaped and potentially recurrent GB single clones to IT, and investigated RNA expression of senescence-associated factors in newly diagnosed vs. recurrent tumors of patients exposed only to the standard therapy [3] as well as of those exposed additionally to IT after the onset of the first recurrence i.e. onset of TMZ resistance.

2. Materials and methods

2.1. Cell culture, drug treatment, siRNA-mediated knockdown and plasmid transfection

The GB cell lines A172 (RRID:CVCL_0131), LN18 (RRID:CVCL_0392), LN229 (RRID:CVCL_0393), LN308 (RRID:CVCL_0394), LN319 (RRID:CVCL_3958), LN428 (RRID:CVCL_3959) were cultivated in Dulbecco's minimal essential medium (DMEM) containing 10 % fetal bovine serum (FBS) in a humidified atmosphere containing 5 % CO_2 at 37°C. The A172 line was purchased from Cell Line Service (Eppelheim, Germany) and the LN229 cells were obtained from LGC Standards (Wesel am Rhein, Germany). All other cell lines (LN18, LN308, LN319 and LN428) were a generous gift from Prof. Michael Weller (University of Zürich, Switzerland). The cell lines were regularly checked for mycoplasm contamination using the VenorGEM classic detection kit (#11–1100, Minerva Biologicals). TMZ was a kind gift of Prof. Geoff Margison (Centre for Occupational and Environmental Health, University of Manchester, United Kingdom). TMZ was solubilized in dimethyl sulfoxide (DMSO), diluted in distilled water immediately before use and administered at a final concentration of 50 μM. IT (CPT-11) was prepared at 20 mg/mL stock solution by the pharmacy of the University Medical Center Mainz, and was used at the final concentration of 5 μM. BV6 inhibitor (targets cellular inhibitor of apoptosis protein 1 and 2 (cIAP1 and cIAP2); CAS 1001600–56–1, Selleckchem) was solubilized in DMSO and used at the indicated concentrations. The p53 inhibitor Pifithrin α (Pthα, P4359, Sigma-Aldrich, St. Louis, MO, USA) was used at 30 μM. For silencing $p21^{CIP1}$, Waf1/Cip1/CDKN1A $p21^{CIP1}$ siRNA (h) (sc-29427, Santa Cruz) was used. For PTEN knockdown, PTEN siRNA (h) (sc-29459, Santa Cruz) was applied. Control human non-silencing siRNA (Silencer Select Predesigned siRNA-Negative Control #1 siRNA; Ambion, Austin, TX, USA) was used as a transfection control. Cells were transfected with siRNAs using Lipofectamine RNAiMAX transfection reagent (Thermo Fisher Scientific). For re-expressing $p14^{ARF}$ or $p16^{INK4A}$, cells were transfected with the pcDNA3-myc-ARF or pCMVp16INK4A, and with pcDNA3 as a mock control, using Effectene Reagent (Qiagen, Hilden, Germany). pCMVp16INK4A was a gift from Bob Weinberg (*Addgene* plasmid #10916; http://n2t.net/addgene:10916; RRID:Addgene_10916) [39]. pcDNA3-myc-ARF was a gift from Yue Xiong (*Addgene* plasmid #19930; http://n2t.net/addgene:19930; RRID:Addgene_19930) [36]. For overexpressing $p21^{CIP1}$, self-made pcDNA3-p21 plasmid was used [40].

2.2. Determination of colony formation, cell death, cell cycle progression, and senescence

For colony formation assay (CFA), 1×10^3 cells were seeded per 6-cm dish and 24 h later exposed to anticancer drugs, as described [41]. Colonies were fixed in methanol and stained with 1.25 % Giemsa/0.125 % crystal violet three weeks after exposure. To determine IT-induced cell death and cell cycle distribution, attached and detached

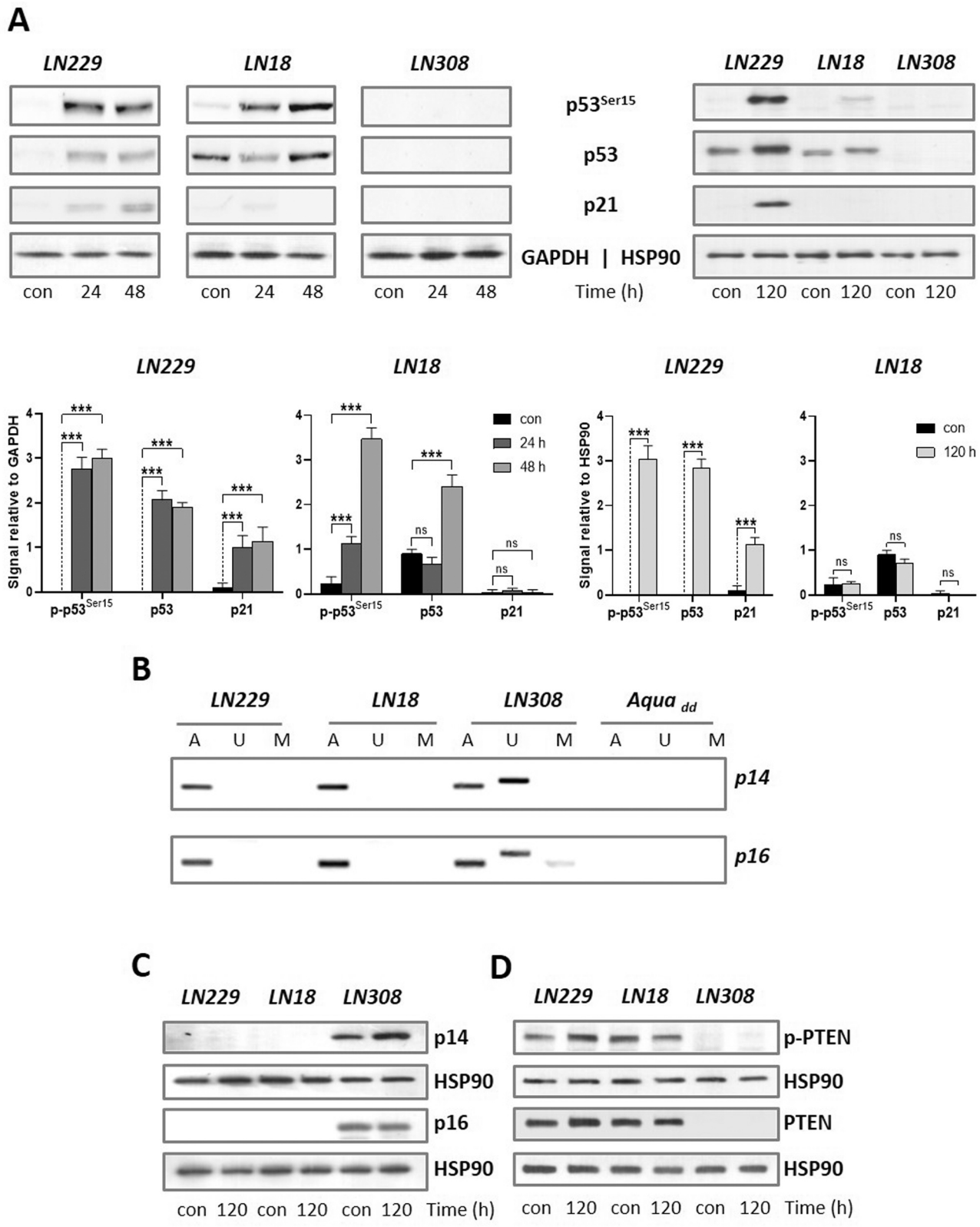

Fig. 1. Protein expression of cell cycle regulators upon drug exposure and methylation-specific PCR. **(A)** GB cell lines LN229, LN18 and LN308 were exposed to 5 μM IT for 24 or 48 h, or 120 h (upper panel). Expression of phosphorylated $p53^{Ser15}$, total p53 and p21 was analyzed by immunoblotting. GAPDH and HSP90 were used as loading controls. A representative blot out of three independent blots is shown. The blots were quantified in relation to the loading control set to 1 (lower panel). Differences between treatment and control (con) were statistically analyzed using Student's *t* test (ns = non-significant, $*p < 0.1$, $**p < 0.01$, $***p < 0.001$). **(B)** Promoter methylation of *p14* and *p16* in untreated LN229, LN18 and LN308 cells was determined by methylation-specific PCR (U = unmethylated; M = methylated). ACTB (A) was used as a positive control and double-distilled water ($Aqua_{dd}$) as a negative primer control. **(C/D)** GB cell lines LN229, LN18 and LN308 were exposed to 5 μM IT for 120 h and expression of p14, p16, phosphorylated PTEN (p-PTEN) and total PTEN was analyzed by immunoblotting. HSP90 was used as loading control. Representative blots out of three independent blots are shown.

cells were collected and stained with PI and analyzed by flow cytometry using BD FACSCanto II, as described [41]. Senescence was measured by senescence-associated β-galactosidase (SA-β-Gal) staining and flow cytometry-based C_{12}FDG staining in attached cells as described [42]. Experiments were repeated at least three times, mean values ± SD are shown.

2.3. Preparation of RNA, cDNA synthesis and quantitative real time PCR (qPCR)

Total RNA was isolated using the Nucleo Spin RNA Kit (Machery and Nagel, Düren, Germany). One μg total RNA was transcribed into cDNA (Verso cDNA Kit, Thermo Scientific) and qPCR was performed using the GoTaq®qPCR Master Mix Protocol (Promega, Madison, USA) and the CFX96 Real-Time PCR Detection System (Biorad, München, Germany). In all experiments, qPCR was performed in technical triplicates, SD shows intra-experimental variation. The analysis was performed using CFX Manager™ Software. Non-transcribed controls were included in each run, expression was normalized to *GAPDH* and *ACTB*; the untreated control was set to one. The specific primers are listed in Table S1.

2.4. RNA isolation from shock-frozen tumor material

The biological material (shock-frozen tissue and FFPE microscope slides of primary and corresponding recurrent GB) and associated data were provided by the *French Glioblastoma Biobank* (FGB, CHU Angers, BRIF n° BB-0033–00093). Disposal of the biological material and the associated data is regulated *via* the Material Transfer Agreement between the Centre Hospitalier Universitaire d'Angers and the University Medical Center of the Johannes Gutenberg-University Mainz. Information letter and patients consent form are provided in French (Annex 3). The positive ethics vote was additionally obtained from the ethics committee at the Rhineland-Palatinate State Medical Association (Application number 2022–16425). Collection, handling, and biobanking of the patients' GB tissue was described in detail [43]. Nucleic acids and proteins were isolated from the frozen material using the kit for the preparation of nucleic acids and proteins from the formalin-fixed paraffin-embedded tissues (Quick-DNA/RNA™ FFPE Mini Prep, Zymo Research). The nucleic acid quality and the concentration were measured at Nano Drop 2000 (Thermo Scientific peQlab). The cDNA synthesis and qPCR were performed as described above.

2.5. Preparation of genomic DNA and methylation-specific PCR (MSP)

DNA was extracted according to standard protocols using phenol-chloroform extraction. Modification of the DNA was performed using the EZ DNA Methylation Kit (Zymo Research). Methylation specific PCR [44] was performed using following primer sequences (5'-3'): $p14^{ARF}$: Meth-up GTGTTAAAGGGCGGCGTAGC, Meth-low AAAACCCTCACTCGC GACGA, Unmeth-up TTTTTGGTGTTAAAGGGTGGTGTAGT, Unmeth-low CACAAAAACCCTCACTCACAACAA; $p16^{INK4A}$: Meth-up TTATTA-GAGGGTGGGGCGGATCGC, Meth-low GACCCCGAACCGCGACCGTAA, Unmeth-up TTATTAGAGGGTGGGGTGGATTGT, Unmeth-low CAACCC-CAAACCACAACCATAA. Specific primers for $p14^{ARF}$ and $p16^{INK4A}$ have been published before [45]. As positive control for the reaction, the ACTB promoter was included. ACTB-up AGGGAGTATATAGGTTGGGGAAGTT, ACTB-low AACACACAATAACAAACACAAATTCAC.

2.6. Preparation of protein extracts and western blot analysis

Whole-cell extracts were prepared as previously described [46]. Primary antibodies were diluted 1:500–1:1000 in 5 % BSA, 0.1 % Tween-TBS and incubated overnight at 4°C. Peroxidase-coupled secondary antibodies were diluted 1:2000 and incubated 2 h at RT. The protein-antibody complexes were visualized by chemo-luminescence using Pierce® ECL Western Blotting Substrate (Thermo Fisher Scientific), and immunodetection was performed using X-ray films and the iBright CL1000 system (Invitrogen). The specific antibodies are listed in Table S2.

2.7. Statistical analysis

The data were statistically evaluated using two-way ANOVA with Bonferroni correction or Student's *t*-test and were expressed as a mean ± SD $*p \leq 0.1$ significant, $**p \leq 0.01$ very significant, $***p \leq 0.001$ highly significant. Statistical analyses were performed using GraphPad Prism version 8 for Windows, GraphPad Software, La Jolla, CA, USA.

3. Results and discussion

3.1. Expression of p53, $p21^{CIP1}$, $p16^{INK4A}$ and $p14^{ARF}$ in model GB cell lines upon IT exposure

To analyze induction of crucial DNA damage response and cell cycle mediating factors, the GB cell lines LN229, LN18 and LN308 were exposed to 5 μM IT. As shown in Fig. 1**A**, LN229 cells induced the total and phosphorylated (transactivating) form of p53 ($p53^{Ser15}$) 24 and 48 h after IT. In parallel, induction of $p21^{CIP1}$ was observed after 24 h, which further increased at later exposure times (48 h), and was still significantly upregulated 120 h after exposure (right panel). LN18 cells expressed mutated p53 in the untreated control (con), hence in the absence of DNA damage. Upon IT exposure, they expressed phosphorylated p53, however, this transactivating signal was insufficient to induce its target, $p21^{CIP1}$, neither at 48 nor at 120 h. The same was true for p53 in mutated LN319 and LN428 lines, not expressing $p21^{CIP1}$ or expressing it to a fairly high level already in the untreated control, respectively (Fig. S1A). In LN308 both p53 alleles are deleted, and thus these cells express neither p53 nor $p21^{CIP1}$ (Fig. 1**A**). Methylation-specific PCR of exon 1α (specific for $p16^{INK4A}$) and exon 1β (specific for $p14^{ARF}$) from the *CDKN2A* promoter showed neither the signal for the methylated nor for the unmethylated $p14^{ARF}$ and $p16^{INK4A}$ in LN229 and LN18 cells (Fig. 1**B**). This shows that the corresponding exon is deleted in those cell lines. This leads to a complete absence of the $p14^{ARF}$ and $p16^{INK4A}$ protein expression in LN229 and LN18 (Fig. 1**C**). On the contrary, in LN308, both, $p14^{ARF}$ and $p16^{INK4A}$ were found unmethylated (Fig. 1**B**); therefore, LN308 cells strongly expressed both proteins (Fig. 1**C**). Of note, $p14^{ARF}$ was slightly induced upon IT exposure, whereas $p16^{INK4A}$ expression remained the same in nonexposed and exposed LN308 cells. Another $p14^{ARF}$/$p16^{INK4A}$ proficient cell line analyzed was LN319; all other lines were negative (for protein expression and MSP, see Fig. S1A/**B**). Apart from the $p21^{CIP1}$, $p14^{ARF}$/$p16^{INK4A}$ status, we also examined expression of the tumor suppressor PTEN, which is deleted in many tumors and crucial for decision of a cell to undergo cell cycle arrest, apoptosis or senescence; loss of PTEN was shown to be connected with induction of cellular senescence without DNA damage [47,48]. Also, DNA damage-induced senescence seems to be facilitated by PTEN loss [49].

LN229 and LN18 expressed phosphorylated and total PTEN upon IT exposure, whereas LN308 were negative (Fig. 1**D**), which is due to a known gene deletion [50]. PTEN expression in additional cell lines is shown in Fig. S1A. Of notice, according to the online data base *DepMap Portal* (https://depmap.org/portal/), LN319 express mutated PTEN, but the mutation is not damaging, meaning PTEN is, in fact, functional.

3.2. Colony formation, induction of cell death and cell cycle distribution in model GB cell lines

To investigate whether expression/absence of these factors impacts the cellular response to IT, colony forming ability was analyzed. As shown in Fig. 2**A** (upper and lower panel), upon IT concentrations > 1 μM, p53/$p21^{CIP1}$ proficient LN229 and A172 lines completely abrogated colony formation. At 3–4 μM IT, LN308 and LN18, as well as

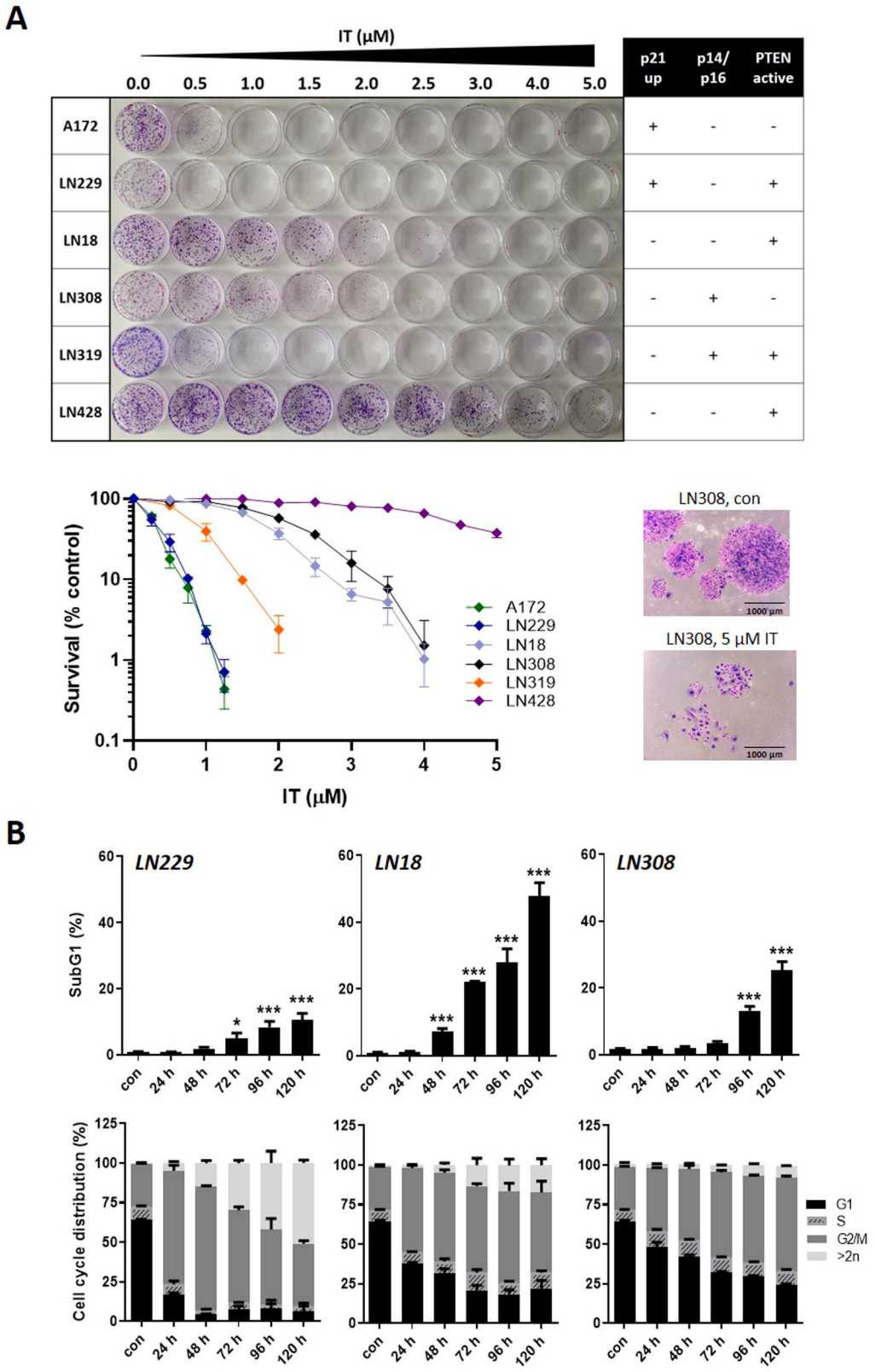

Fig. 2. Impact of IT exposure on survival, cell death and cell cycle regulation in GB cell lines. **(A)** A172, LN229, LN18, LN308, LN319 and LN428 cells with different profiles regarding p21 induction (p21 up), p14/p16 and PTEN status were treated with IT in varying concentrations for two weeks (upper panel). Survival was calculated by normalization of assessed colonies to the respective untreated control (lower panel). A representative microscopy picture of observed microcolonies of LN308 is shown in the lower right compared to untreated control colonies. **(B)** Cell death and cell cycle distribution of LN229, LN18 and LN308 cells were measured after treatment with 5 μM IT for 24–120 h by flow cytometry using PI staining. Experiments were performed in triplicates. Differences between treatment and control (con) were statistically analyzed using Student's *t* test (non-labeled = non-significant, $*p < 0.1$, $**p < 0.01$, $***p < 0.001$).

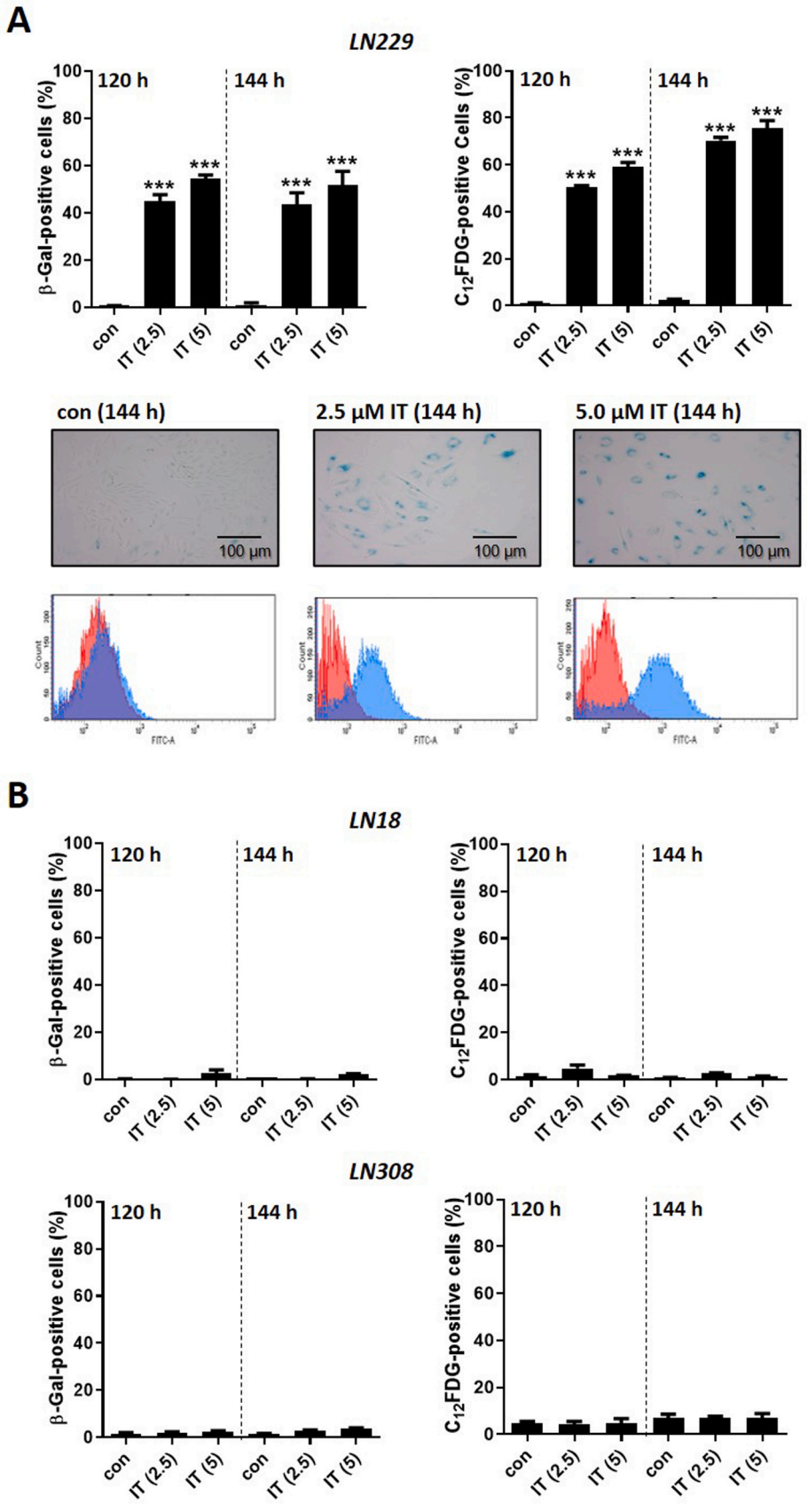

(caption on next page)

Fig. 3. Senescence induction of GB cell lines exposed to IT. **(A)** LN229 were treated with IT (2.5 or 5 μM) for 120 or 144 h and senescence induction measured by either β-galactosidase staining assay or C_{12}FDG flow cytometric assay. Representative microscopy pictures for the β-galactosidase staining assay are shown as well as representative graphs for evaluation of the C_{12}FDG flow cytometric assay (red = non-senescent control cells; blue = treated cells). **(B)** LN18 and LN308 cells were treated with IT (2.5 or 5 μM) for 120 or 144 h and senescence induction measured by either β-galactosidase staining assay or C_{12}FDG flow cytometric assay. Experiments were performed in triplicates. Differences between treatment and control (con) were statistically analyzed using Student's *t* test (non-labeled = non-significant, $^{*}p < 0.1$, $^{**}p < 0.01$, $^{***}p < 0.001$).

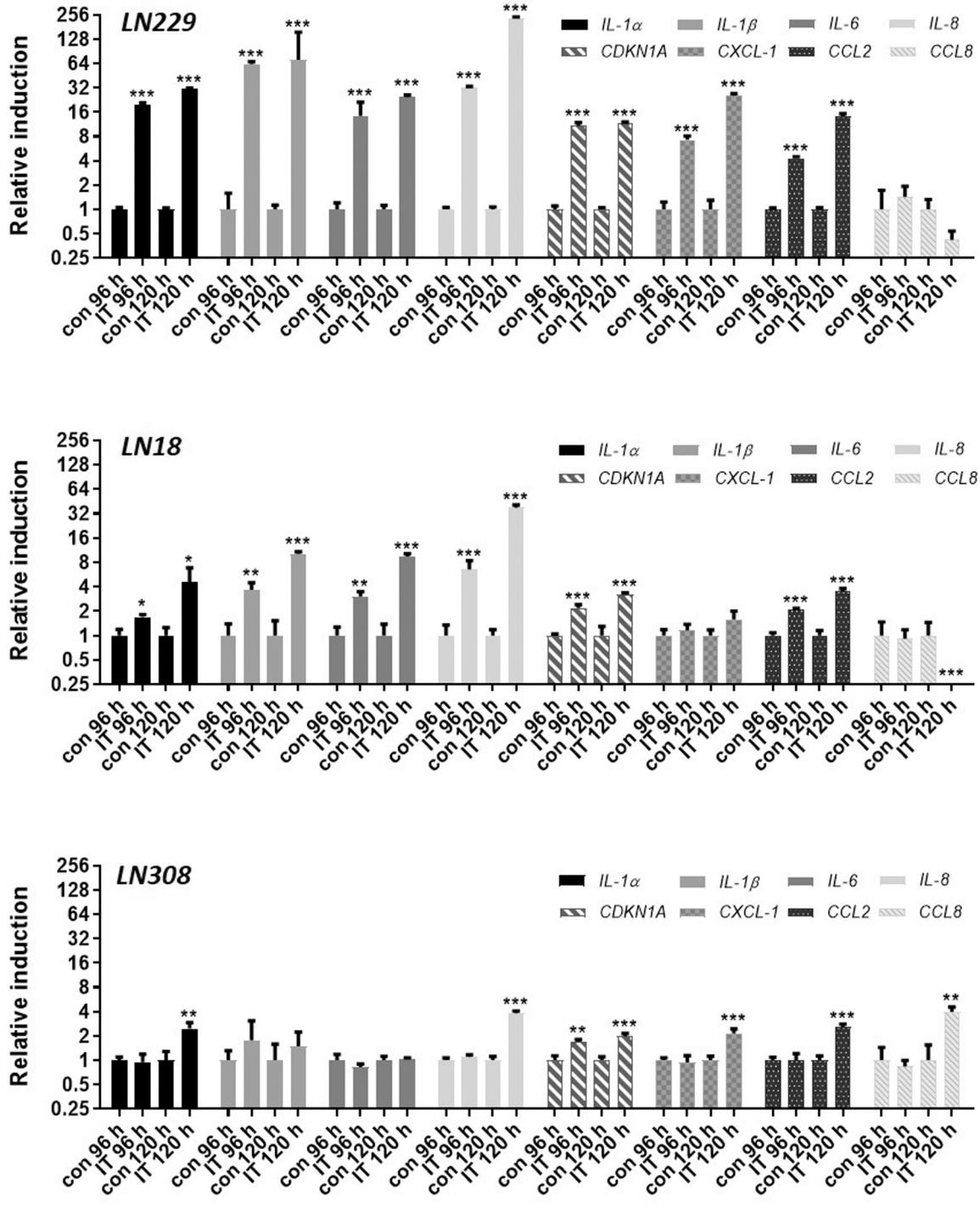

Fig. 4. Transcriptional regulation of SASP factors upon IT treatment. Expression of SASP factors (*IL-1α*, *IL-1β*, *IL-6*, *IL-8*, *CDKN1A*, *CXCL-1*, *CCL2*, *CCL8*) in LN229, LN18 and LN308 cells after exposure to 5 μM IT for 96 or 120 h was assessed by real-time qPCR. ACTB and GAPDH were used as internal loading control. Experiments were performed in triplicates. Differences between treatment and control (con) were statistically analyzed using Student's *t* test (non-labeled = non-significant, $^{*}p < 0.1$, $^{**}p < 0.01$, $^{***}p < 0.001$).

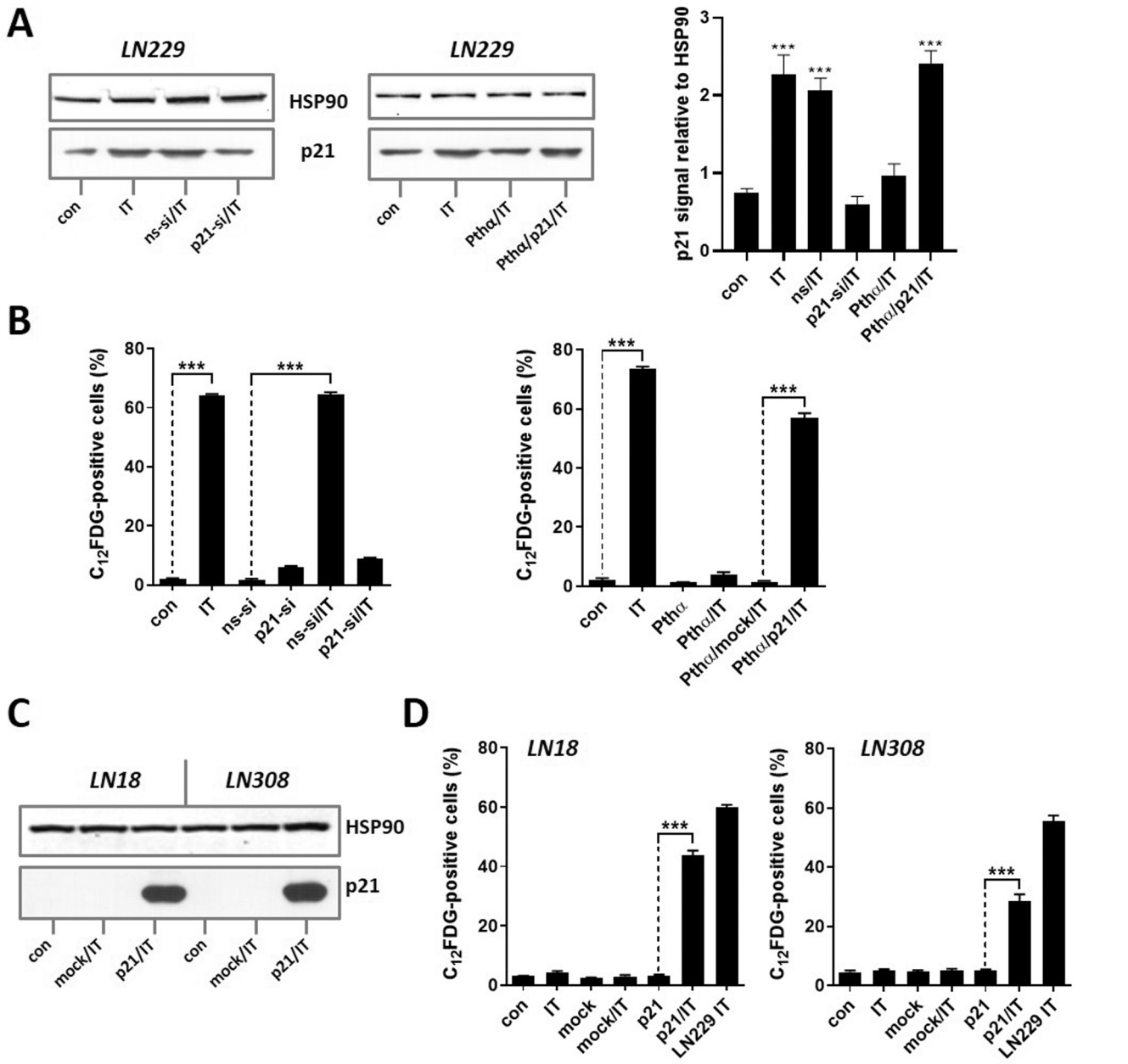

Fig. 5. Modulation of p21 expression and induction of senescence. **(A)** LN229 cells were exposed to 5 μM IT, or were transfected with non-silencing siRNA (ns-si) or p21-specific siRNA (p21-si) at 20 nM each, and 24 h later exposed to 5 μM IT for 120 h. Alternatively, the cells were pre-treated with Pifithrin α (30 μM Pthα) and 24 h later treated with 5 μM IT for 120 h, or were Pthα-pre-treated and 6 h later transfected with the recombinant plasmid expressing *p21*-cDNA (pcDNA3-p21), and 18 h later exposed to 5 μM IT for 120 h. Expression of p21 was determined by immunoblotting. HSP90 was used as loading control. con, non-transfected and non-exposed cells. Representative blots out of three independent blots are shown. The blots were quantified in relation to the loading control set to 1 (right panel). **(B)** LN229 cells were exposed to 5 μM IT, or were transfected with non-silencing siRNA (ns-si) or p21-specific siRNA (p21-si) at 20 nM each, and 24 h later exposed to 5 μM IT for 120 h. Alternatively, the cells were pre-treated with 30 μM Pthα and 24 h later treated with 5 μM IT for 120 h, or were Pthα-pre-treated and 6 h later transfected with the recombinant pcDNA3-p21 plasmid or mock-transfected, and 18 h later exposed to 5 μM IT for 120 h. con, non-transfected and non-exposed cells. Senescence was determined by flow cytometric analysis using C_{12}FDG. **(C)** LN18 and LN308 cells were mock- or pcDNA3-p21-transfected, and 24 h later exposed to 5 μM IT for 120 h. Expression of p21 was determined by western blot analysis. HSP90 was used as loading control. con, non-transfected and non-exposed cells. Representative blots out of three independent blots are shown. **(D)** LN18 and LN308 cells were mock- or pcDNA3-p21-transfected, and 24 h later exposed to 5 μM IT for 120 h. Senescence was determined by flow cytometric analysis using C_{12}FDG. As positive control, LN229 cells were exposed to 5 μM IT for 120 h (LN229 IT). Experiments were performed in triplicates. Differences between treatment and respective control were statistically analyzed using Student's *t* test (non-labeled = non-significant, $*p < 0.1$, $**p < 0.01$, $***p < 0.001$).

other p53/p21^{CIP1} inactive lines (for protein expression, see Fig. S1A) still formed few (0.5 %) colonies. At the concentration above 4 μM IT, the clonal growth was completely abolished in all cell lines, except for LN428, which was highly resistant. In addition, LN308 exhibited a significant number of microcolonies (lower right panel). To further examine whether these significant differences in the clonal survival are based on differences in induction of cell death, we determined the SubG1 fraction in our model cell lines. At the highest concentration used (5 μM IT) and exposure for 120 h, LN229 cells exhibited, at maximum, a death frequency of only 10 %, whereas approx. 50 % of LN18 and

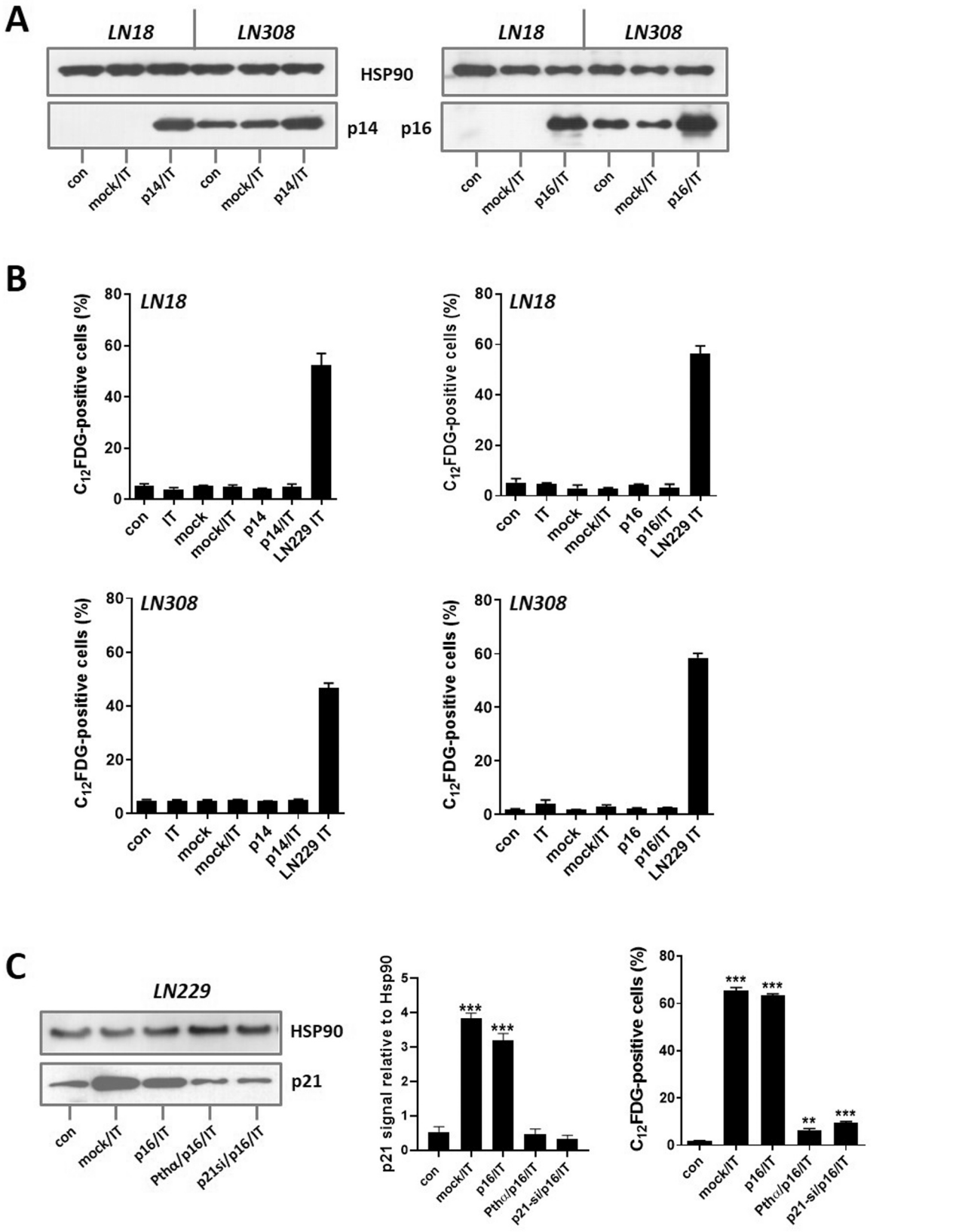

(caption on next page)

Fig. 6. Modulation of p14/p16 expression and determination of senescence. **(A)** LN18 and LN308 cells were mock-transfected or transfected with plasmids expressing p14ARF and p16INK4A, and 24 h later exposed to 5 μM IT for 120 h. Expression of p14 and p16 was determined by immunoblotting. HSP90 was used as loading control. con, non-transfected and non-exposed cells. Representative blots out of three independent blots are shown. **(B)** LN18 and LN308 cells were mock-transfected or transfected with plasmids expressing p14ARF and p16INK4A, and 24 h later exposed to 5 μM IT for 120 h. Senescence was determined by flow cytometric analysis using C_{12}FDG. As positive control, LN229 cells were exposed to 5 μM IT for 120 h (LN229 IT). **(C)** LN229 cells were mock-transfected or transfected with plasmid expressing p16INK4A, and 24 h later exposed to 5 μM IT for 120 h. Alternatively, LN229 cells were pre-treated with 30 μM Pthα, or transfected with p21-siRNA (20 nM), 6 h later transfected with p16INK4A-expressing plasmid, and 18 h later exposed to 5 μM IT for 120 h. Expression of p21 was determined by western blot analysis. HSP90 was used as loading control. con, non-transfected and non-exposed cells. A representative blot out of three independent blots is shown (left panel). The blots were quantified in relation to the loading control set to 1 (middle panel). Senescence was determined by flow cytometric analysis using C_{12}FDG (right panel). Experiments were performed in triplicates. Differences between treatment and respective control were statistically analyzed using Student's *t* test (non-labeled = non-significant, $*p < 0.1$, $**p < 0.01$, $***p < 0.001$).

25–30 % of LN308 cells died (Fig. 2**B**). Thus, induction of cell death *per se* cannot be attributed to those great differences in colony formation among those GB lines. This particularly pertains to LN229 cells, with only 10 % of cells in SubG1 fraction, despite a huge proliferation arrest in the CFA. Next, we determined the cell cycle distribution. As already published by us for exposure of GB cells to TMZ [8,9], LN229 exhibited a significant fraction of cells in G2/M and > 2 n (polyploid cells); at 5 μM IT, both fractions together comprised 90 % (the SubG1 fraction was excluded). At 2.5 and 5 μM IT (96 h), a significant fraction of LN18 and LN308 was in G2/M but, in comparison to LN229, much less cells were

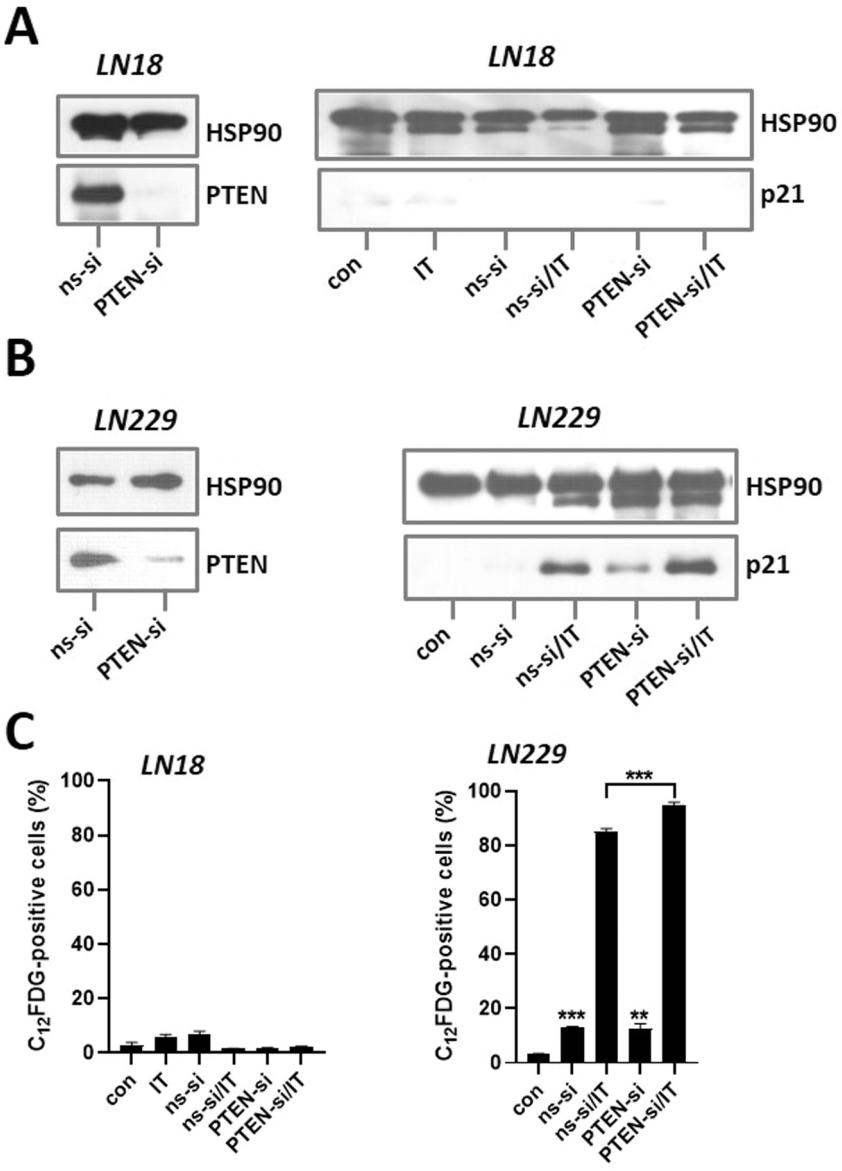

Fig. 7. Modulation of PTEN expression and determination of senescence. LN18 cells **(A)** and LN229 cells **(B)** were transfected with non-silencing siRNA (ns-si) or PTEN-specific siRNA (PTEN-si) at 20 nM each, and 24 h later exposed to 5 μM IT for 120 h. Expression of PTEN after transfection (left panel) and p21 after treatment (right panel) were assessed by immunoblotting. HSP90 was used as loading control. **(C)** Senescence induction was measured by flow cytometry using C_{12}FDG. Experiments were performed in triplicates. Differences between treatment and respective control were statistically analyzed using Student's *t* test (non-labeled = non-significant, $*p < 0.1$, $**p < 0.01$, $***p < 0.001$).

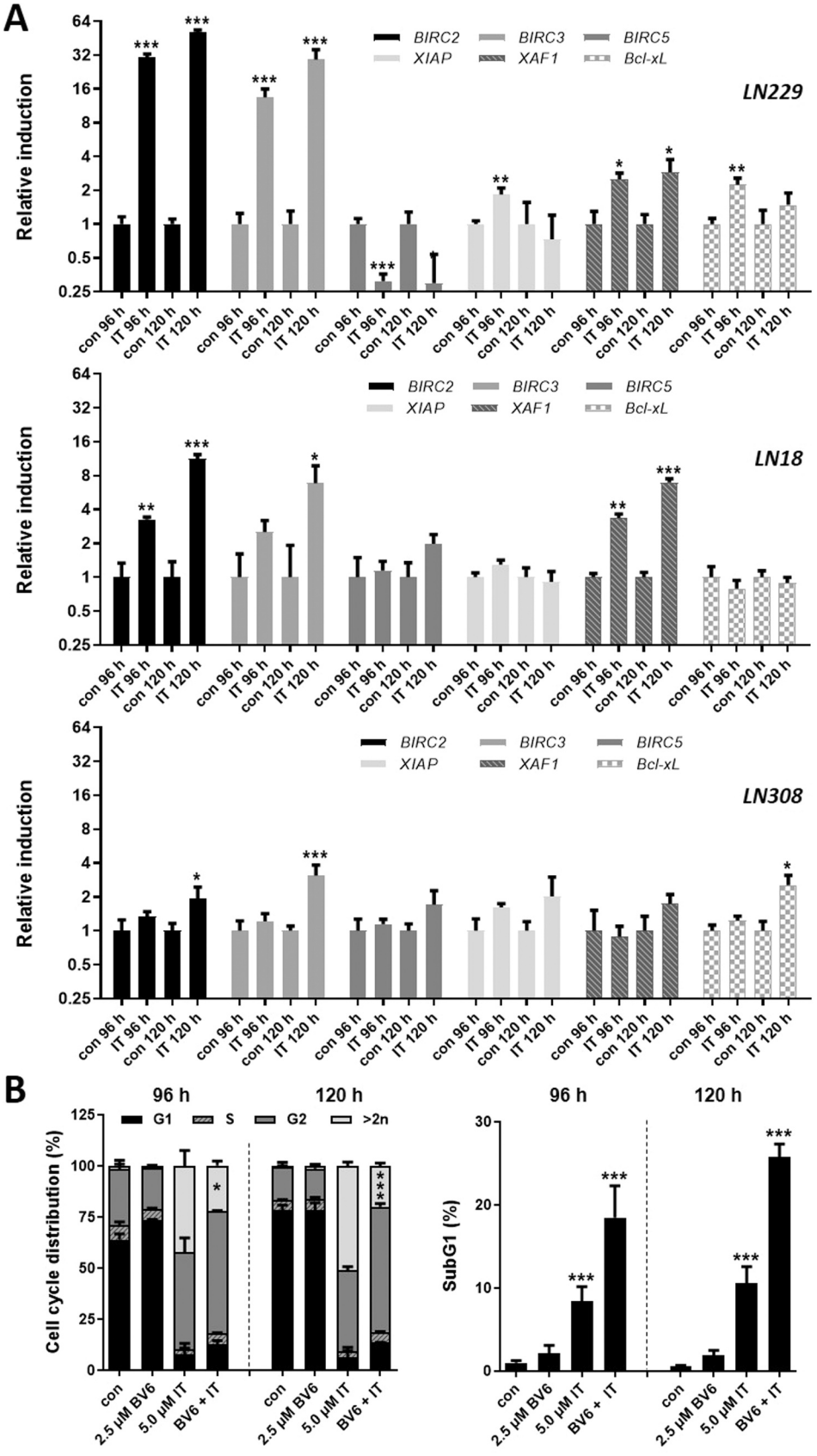

(caption on next page)

Fig. 8. Transcriptional regulation of SCAP factors and senolytic effect of BV6 on IT-treated cells. **(A)** Expression of SCAP factors (*BIRC2*, *BIRC3*, *BIRC5*, *XIAP*, *XAF1*, *Bcl-xL*) in LN229, LN18 and LN308 cells after exposure to 5 μM IT for 96 or 120 h was assessed by real-time qPCR. *ACTB* and *GAPDH* were used as internal loading control. **(B)** Cell cycle distribution (left graph) and cell death (right graph) of LN229 cells treated with 2.5 μM BV6, 5 μM IT or a combination of BV6 and IT for 96 or 120 h were measured by flow cytometry using PI staining. Experiments were performed in triplicates. Differences between treatment and control (con) and in the case of cell cycle distribution differences between the polyploid cell fractions of combination treatment and IT exposure were statistically analyzed using Student's *t* test (non-labeled = non-significant, $*p < 0.1$, $**p < 0.01$, $***p < 0.001$).

polyploid (Fig. S2A). The same was true for the time-dependent cell cycle distribution upon 2.5 μM IT (Fig. S2B). Although not upregulating $p21^{CIP1}$, the p53-mutated LN319 cells, which are the slowest of all used GB lines, were strongly arrested in G2/M and after late times underwent significant cell death (Fig. S2C).

3.3. Induction of cellular senescence and upregulation of SASP in model GB cell lines

To substantiate that polyploid cells hint to induction of cellular senescence, as published by us for exposure of GB cells to TMZ [8,9], GB lines were exposed to 2.5 and 5 μM IT, respectively, and SA-β-Gal-positive as well as C_{12}FDG-positive cells were determined. Whereas a fraction of up to 80 % LN229 cells was senescent after a 144h-exposure to IT (Fig. 3**A**), neither LN18 nor LN308 underwent cellular senescence (Fig. 3**B**). Similar to the published data with TMZ [9], p53/$p21^{CIP1}$–proficient A172 cells entered significant senescence upon IT as well; they exhibited even a stronger blue staining marking β-galactosidase activity (Fig. S3), as compared to LN229 cells. LN428, which were highly resistant to IT in CFA, entered neither cell death (Fig. S2C) nor senescence (Fig. S3). To further verify the results obtained by β-Gal and C_{12}FDG staining, we next measured the SASP activation, which is characterized by the induction and secretion of different cytokines and represents a clinically relevant mechanism affecting the outcome of cancer therapy [51,52]. In order to analyze whether IT can induce the SASP in GB lines, the time-dependent expression of different components of the SASP was analyzed (Fig. 4). As expected, the strongest upregulation of the SASP factors was observed in LN229 cells. However, also LN18 cells, which did not undergo β-Gal-mediated senescence, upregulated SASP markers to some extent, e.g. IL-8. Generally seen, LN308 cells exhibited the weakest SASP response. Altogether, those findings indicate that the GB lines with a pronounced induction of $p21^{CIP1}$ (LN229, A172) undergo a stable cell cycle arrest which transforms into senescence, meaning those cells cannot form colonies, as shown in Fig. 2**A/B**. Thus, senescence prevails, it is the main trait for sensitivity, not cell death. The GB lines, which did not undergo senescence but rather cell death (LN18), or were strongly arrested in the cell cycle and very lately died (LN319) showed a less steep curve (Fig. 2**B**). This goes along with the data showing that p53 disruption profoundly alters response of human GB cells to TOP1 inhibitors [29].

3.4. $p21^{CIP1}$ is the rate-limiting factor and sufficient to induce senescence of GB cells upon IT exposure

To examine whether genetic silencing of $p21^{CIP1}$ and/or pharmacological inhibition of p53 is sufficient to abolish IT-induced senescence of LN229 cells, the cells were transfected with $p21^{CIP1}$-siRNA or exposed to Pifithrin α (Pthα), the inhibitor of the p53 transactivating activity (Fig. 5**A**), and afterwards treated with IT. Both inhibiting approaches led to a complete abrogation of IT-induced β-galactosidase-mediated senescence (Fig. 5**B**). When LN229 cells were treated with Pthα and shortly thereafter transfected with the plasmid expressing $p21^{CIP1}$-cDNA, IT-induced senescence of LN229 cells could be significantly rescued (Fig. 5**B**, right panel, last column). The same could be observed in A172 cells (Fig. S4A/**B**).

Ectopic expression of $p21^{CIP1}$ in LN18 and LN308 cells (Fig. 5**C**), led to a significant increase in C_{12}FDG-positive cells that were exposed to IT (Fig. 5**D**), again underlying sustained DDR accompanied by $p21^{CIP1}$ activity is crucial for induction of cellular senescence in GB cell model. In contrast, upon $p14^{ARF}$-cDNA (Fig. 6**A**, left panel) or $p16^{INK4A}$-cDNA (Fig. 6**A**, right panel) transfection, neither LN18 nor LN308 cells became senescent (Fig. 6**B**). *Nota bene*, immunodetection was performed with much lower amount of the cell extract to better observe the ectopic expression from the plasmid, since LN308 cells express already a high amount of $p14^{ARF}$ and $p16^{INK4A}$ (see Fig. 1**C**). This once again excludes $p14^{ARF}$ and $p16^{INK4A}$ to be rate-limiting and essential for GB cells to enter IT-triggered senescence. In addition, ectopic expression of $p16^{INK4A}$ in LN229 cells (Fig. 6**C**, left panel) was unable to rescue IT-induced senescence of cells priorly treated with Pthα or $p21^{CIP1}$-siRNA (Fig. 6**C**, right panel, last two bars), once again supporting the fact that $p16^{INK4A}$ does not play an essential role in this context.

Also, knockdown of PTEN in LN18 (Fig. 7**A,** left panel) cells had no impact on senescence (Fig. 7**C,** left panel). LN18 cells underwent cell death upon IT alone and combined PTEN-si/IT exposure (Fig. S5). PTEN knockdown in LN229 cells (Fig. 7**B,** left panel) slightly increased senescence frequency after IT exposure (Fig. 7**C,** right panel), indicating a reinforcing but not essential role regarding senescence induction. Knockdown of PTEN in LN229 led to induction of $p21^{CIP1}$ on its own (Fig. 7**B,** right panel). While this resulted only in a mild senescence induction, which was already observed in the non-silencing siRNA transfected cells and may be a side-effect of transfection, the increased $p21^{CIP}$ induction may explain the strengthened effect of IT exposure (Fig. 7**C,** right panel). As described previously for other cell types, e.g. BJ-T and MCF7 cells, PTEN knockdown induced $p21^{CIP1}$, and in some cases, senescence through activation of the PI3K/AKT pathway, mTORC1 and subsequent phosphorylation of p53 [47,53]. The results in our model suggest that transient $p21^{CIP1}$ induction by PTEN loss alone, i.e., without DNA damage, is not sufficient to induce senescence.

3.5. Upregulation of SCAP factors in model GB cell lines and targeting of SCAPs for senolysis

In order to analyze whether IT induces the senescent cell anti-apoptotic pathways (SCAPs) factors, the time-dependent expression of different anti-apoptotic factors was analyzed by real-time qPCR (Fig. 8**A**). LN229 cells exhibited a more than 32-fold induction of *BIRC2* (encodes cIAP1), *BIRC3* (encodes cIAP2) and a strong repression of *BIRC5* (encodes Survivin). This pronounced transcriptional repression of the *BIRC5* gene with concomitant *CDKN1A/*$p21^{CIP1}$ upregulation implicates that the cells are significantly compromised in their proliferation capacity, undergoing senescence [54–56]. This repression was not observed in LN18 and LN308 cells. Interestingly, at later time points (120 h), LN18 cells upregulated (8-fold) *BIRC2* and *BIRC3* but did not show repression of *BIRC5*, whereas, at the same time, they significantly upregulated *XAF1*, a pro-apoptotic counterpart of Survivin. This goes along with a significant apoptosis induction in those cells. In order to investigate whether, in analogy to TMZ, cellular effects of IT in LN229 cells, such as the G2/M-arrest and polyploidy, could be modulated by compounds targeting SCAPs, and thus, introducing senolytic effects [57, 58], we combined the cIAP1/cIAP2 inhibitor BV6 with IT. Being a second mitochondria-derived activator of caspases (SMAC) mimetic, BV6 acts in a pro-apoptotic way. Since particularly cIAP1 and cIAP2 are found overexpressed in GB cells undergoing therapy-induced senescence (e.g., under TMZ exposure), targeting cellular IAPs might be used as a senolytic approach [57]. After exposure for 96–120 h, a significant senolytic effect of BV6 was observed. Thus, the polyploid fraction of

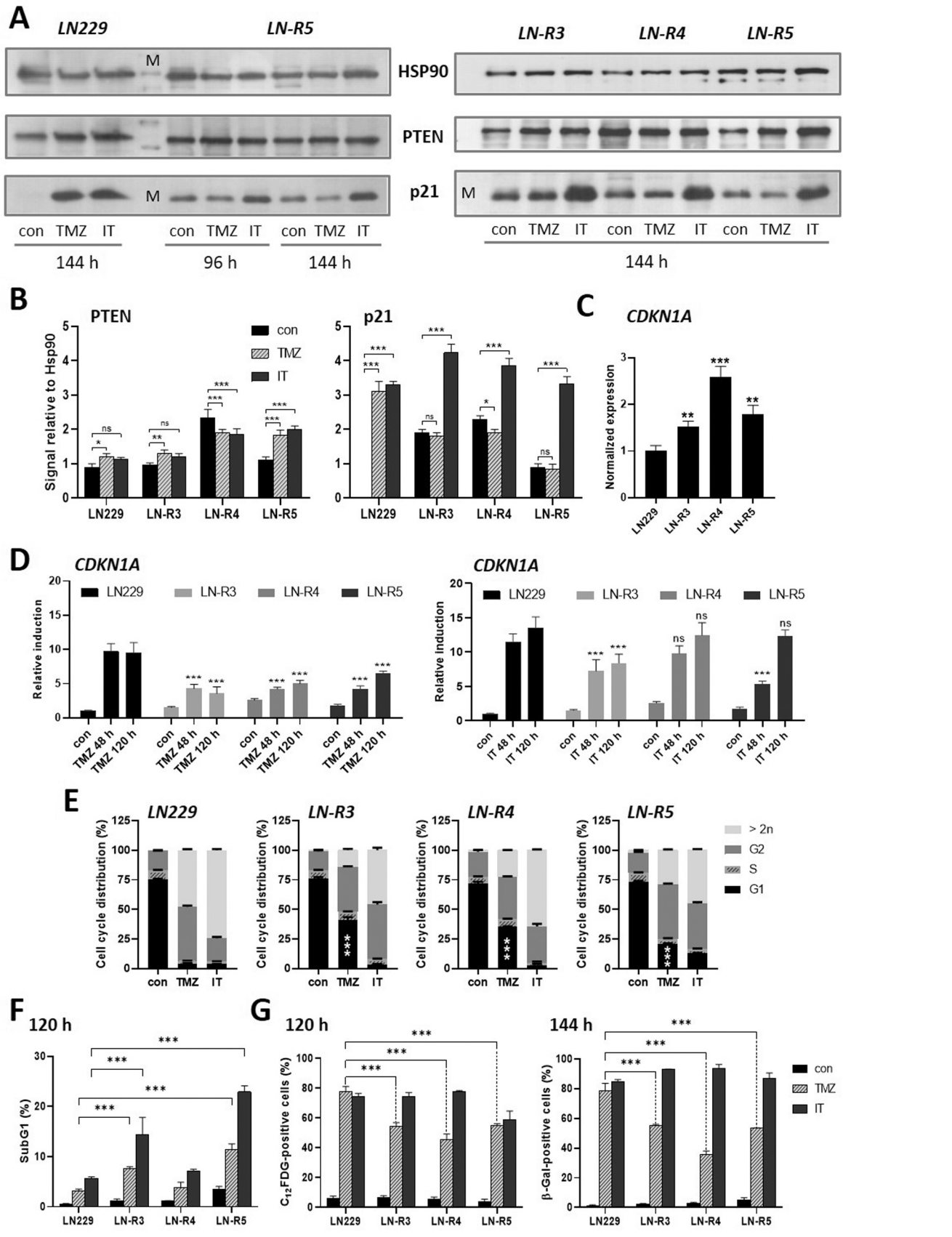

(caption on next page)

Fig. 9. Analysis of potentially recurrence forming clones upon drug treatment. **(A)** LN229 cells and R-clones (LN-R3, LN-R4 and LN-R5) were treated with TMZ (50 μM) or IT (5 μM) for 96 or 144 h and expression of PTEN and p21 detected by immunoblotting. HSP90 was used as internal loading control (M = marker). A representative blot out of three independent blots is shown. **(B)** Signals of immunoblotting were quantified in relation to the loading control set to 1. **(C)** mRNA expression of *CDKN1A* was measured by real-time qPCR in untreated LN229 cells and R clones. **(D)** LN229 cells and R clones were treated with either 50 μM TMZ (left panel) or 5 μM IT (right panel) for 48 or 120 h. Real-time qPCR was used to assess relative induction of *CDKN1A* normalized to the untreated LN229 control (con). Significance indicates differences between treated R-clones and accordingly treated LN229 cells statistically analyzed using two-way ANOVA. Cell cycle distribution **(E)** and cell death **(F)** were measured by flow cytometry using PI staining after treatment of LN229 cells or R clones for 120 h with either TMZ (50 μM) or IT (5 μM). Significance indicates differences between treated R clones and accordingly treated LN229 cells statistically analyzed using Student's *t* test. **(G)** Senescence induction was assessed by either C_{12}FDG flow cytometric assay after 120 h or β-Galactosidase staining assay after 144 h treatment with either 50 μM TMZ or 5 μM IT. Experiments were performed in triplicates. Differences between treatment and control (con) or corresponding LN229 treatment were statistically analyzed using Student's *t* test (non-labeled/ns = non-significant, $*p < 0.1$, $**p < 0.01$, $***p < 0.001$). In **E** only differences in the G1 fraction were analyzed by Student's *t* test.

cells, contributing to senescence of LN229 cells was reduced (Fig. 8**B**, left panel) and cell death was induced, showing more than additive effects (Fig. 8**B**, right panel). Similar results were observed in A172 cells (Fig. S6A/**B**).

3.6. Senescence-escaped TMZ-resistant GB clones can be re-sensitized to IT

To examine whether IT can target TMZ-escaped GB cells, we established a set of cell clones (R-clones LN-R3, LN-R4 and LN-R5) derived from LN229 cells that either evaded or escaped from senescence after one application of 50 μM TMZ for 3–4 weeks. We showed in our previous studies that TMZ predominantly induces senescence and not cell death [8,9,57]. Senescence was shown to be already induced at lower TMZ concentrations (10 and 25 μM), which shows that these concentrations are sufficient to induce G2-arrest and polyploidy, and are nearly completely blocking clonogenic survival [8]. Additionally, the clonogenic survival of U87MG, LN229 and A172 glioma cell lines was reduced to approx. 20 % at ≥ 5 μM TMZ and completely abolished at 15 μM TMZ [9,57], indicating also concentrations that are achievable in the cerebrospinal fluid abrogate proliferation. Moreover, one should keep in mind that in *in vitro* experiments higher concentrations are often necessary, since established cell lines are more robust and not as responsive as cells *in vivo*. Here we used a single application of 50 μM TMZ to be able to simultaneously monitor induction of senescence and cell death, and, in addition, to generate not too many survivors (R-clones), and, also, to possibly avoid cross-resistance to IT. For such tumor clones, it is to assume they might form recurrences and are partially resistant to the corresponding drug (e.g. to TMZ), but might not be cross-resistant to other anticancer drugs (e.g. IT in our experiments).

Our data show that the $p21^{CIP1}$ protein expression was strongly upregulated in untreated R-clones, in comparison to the marginal expression in untreated LN229 cells (Fig. 9**A** and Fig. 9**B** for quantification). Accordingly, also the expression of *CDKN1A* was upregulated in the R-clones, in comparison to the expression in parental LN229 cells as revealed by real-time qPCR (Fig. 9**C**). Furthermore, $p21^{CIP1}$ protein expression could not be induced after exposure to 50 μM TMZ, but was strongly induced upon exposure to 5 μM IT (Fig. 9**A** and Fig. 9**B** for quantification). Again, the R-clones also showed a dampened response to TMZ regarding *CDKN1A* induction (Fig. 9**D,** left panel), while exposure to IT led to a higher induction of *CDKN1A*, which was comparable to parental LN229 cells (Fig. 9**D**, right panel). Opposite to $p21^{CIP1}$, a weak induction was observed for PTEN on protein level (Fig. 9**A** and Fig. 9**B** for quantification) in the original LN229 cells and the R-clones. Importantly, in contrast to TMZ, IT treatment led to a pronounced G2/M-arrest accompanied by β-Gal positivity, reminiscent of the senescence phenotype (Fig. 9**E**). Moreover, upon IT treatment, a higher fraction of cells responded with induction of cell death (Fig. 9**F**) and senescence after 120 and 144 h (Fig. 9**G**). We also determined senescence at earlier time points (48 and 72 h) and lower concentrations of TMZ and IT (Fig. S7A). Also, under these conditions R-clones were less sensitive to TMZ compared to LN229 cells, which was not the case for IT. Analysis of colony forming ability showed that R-clones were still highly sensitive to treatment with IT, forming colonies only until 1.5 μM, while R-clones still consistently formed colonies at 15 μM TMZ, with LN-R5 showing a survival frequency of about 21 % (Fig. S7B).

Finally, we analyzed the expression of multiple SASP and SCAP factors (e.g., Interleukins *IL-1α*, *IL-1β*, *IL-8* and IAPs *BIRC2*, *BIRC3*) in LN229 cells and R-clones. The expression was differently modulated. Here, we want to highlight the normalized expression of the pro-apoptotic factor *XAF1* in LN-R5, which was 80-fold higher than in LN229 cells, respectively (Fig. S8), and might partially explain the higher amount of cell death induced by IT.

3.7. Patients with recurrences receiving IT therapy show prolonged delay to surgery for recurrence

The results in R-clones let assume that in patients, TOP1-based recurrence therapy might be superior to the repeated TMZ therapy. To address this point, we received 13 recurrence samples of GB patients together with the respective primary tumors from the *French Glioblastoma Biobank* (FGB). Based on the clinical data, we identified three patients who were given additional therapy options between the Stupp protocol and surgery for recurrence (Fig. 10**A**). Upon onset of recurrence, these patients were treated with IT (Campto) plus the anti-angiogenic drug Bevacizumab (Avastin; monoclonal antibody against the vascular endothelial growth factor) (Patient 7) or with TMZ (3 cycles) and IT (plus Bevacizumab) (Patient 9). The time between the onset of recurrence and the surgery for recurrence was 553 days, and 351 days, respectively. In comparison, e.g., a male patient of similar age, receiving no additional therapy to Stupp, had a delay to surgery for recurrence of only 43 days (Fig. 10**A**). In another patient, who received Bevacizumab (Patient 12), the time between the onset of recurrence and the surgery for recurrence was 113 days. We excluded Patient 5 from further analysis due to a young age (28 years at diagnosis) and ketogenic diet during therapy.

We are aware that the number of only twelve analyzed patient samples is relatively low, but nevertheless a direct comparison of recurrences to respective (paired) newly diagnosed tumors is much more meaningful than comparing random recurrences to primary tumors, as is the case in publicly available databases (https://www.cbioportal.org/study/summary?id=gbm_tcga_pan_can_ atlas_2018 [uses Glioblastoma Multiforme TCGA PanCancer data; UID: 10414]).

By means of real-time qPCR we analyzed expression levels of SASP and SCAP factors, DNA repair genes and cell cycle inhibitors in the recurrence sample of a patient (referred to as "Rec" in Fig. 10**B**) and set those into relation to the levels in the primary tumor of this very patient. We next looked for similarities and curated two clusters (1 and 2) of recurrences that seemed to behave similarly (Fig. 10**B**). Importantly, *PTEN* mRNA was upregulated in all patients of Cluster 1 (4 patients), whereas *CDKN1A* was downregulated. Opposite, *PTEN* mRNA was down-regulated in all patients of Cluster 2 (4 patients), whereas *CDKN1A* was up-regulated in 3 patients, which coincides with the findings by us (this work) and others, where PTEN loss led to an induction of $p21^{CIP1}$ [47,53,59]. Three patients showed a mixture of Cluster 1 and 2. Of note, Patient 12, who only received Bevacizumab treatment without concomitant TMZ or IT, was among them. Finally, patient 13 showed no differences between primary tumor and

A

Patient No.	Sex	Age	Therapy after initial surgery (max. safe resection)	Additional therapy between Stupp and surgery for recurrence	Delay between onset and surgery for recurrence (d)
1	m	64	Stupp	-	36
2	f	52	Stupp	-	56
3	f	65	Stupp	-	30
4	m	72	Stupp	-	41
5	m	28	Stupp	-	23
6	f	54	Stupp	-	6
7	m	53	Stupp	IT + Bevacizumab	553
8	m	51	Stupp	-	43
9	f	63	Stupp	TM Z+ IT + Bevacizumab	351
10	f	44	Stupp	-	3
11	m	66	Stupp	-	26
12	m	60	Stupp	Bevacizumab	113
13	m	59	Stupp	-	15

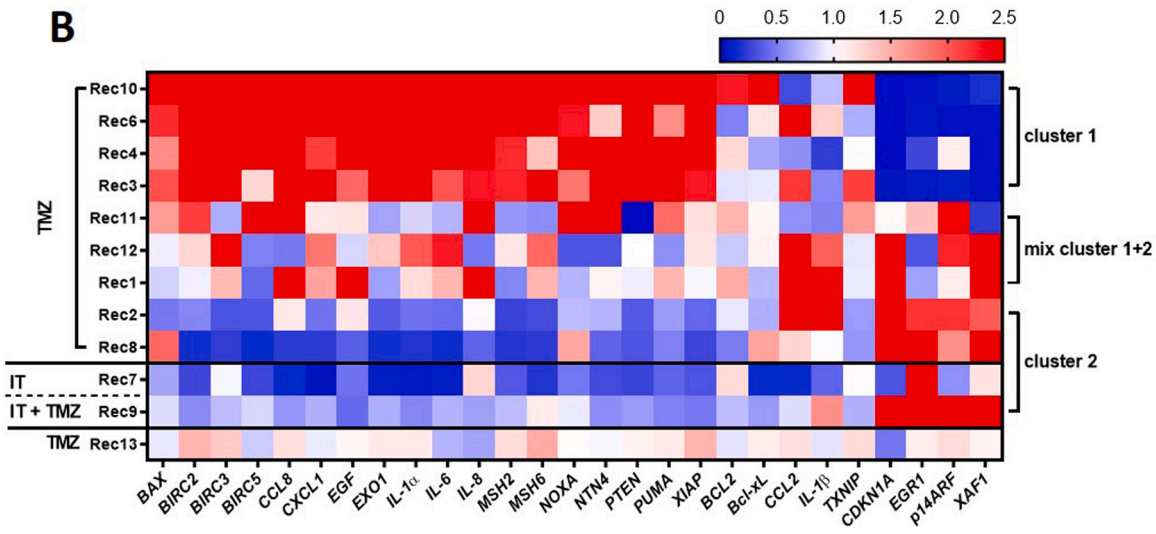

Fig. 10. Analysis of GBM patient tumor samples. **(A)** Sample pairs of primary tumor and respective recurrence of 13 GBM patients, who all received first-line treatment (Stupp protocol) after initial surgery, were obtained from the FGB and classified by sex, age at diagnosis, additional therapy between Stupp protocol and surgery for recurrence and the time (delay) between onset and surgery for recurrence. **(B)** The RNA of tumor samples was analyzed by real-time qPCR and expression levels in the recurrence (Rec) sample normalized to the respective primary tumor set to 1. Two clusters (1 and 2) of samples showing similar expression patterns in the analyzed genes were curated. Type of treatment between onset of recurrence and surgery for recurrence is indicated for each patient (TMZ and/or IT). Three samples (Rec11, Rec 12 and Rec 1) which showed a mixed pattern were classified as "mix cluster 1+2".

recurrence at all. Interestingly, unlike the other patients, this patient showed no positive immunohistochemistry staining for p53 (carried out by the FGB).

It was described that cells, which escape from senescence, e.g. by downregulation of p53 with simultaneous low levels of $p16^{INK4A}$, can retain the SASP [60,61]. This would coincide with the expression profiles of cluster 1, where many SASP factors were commonly upregulated, while an increase of *CDKN1A* was not observed. This finding drives our assumption that recurrences of this cluster may have derived from cells which have initially undergone senescence during standard therapy but then escaped from senescence and started to proliferate again. For several cancer model cell lines, senescence escape has already been described and recently summarized [62], which underlines the theory of recurrences potentially deriving from once senescent cells [63]. One can only hypothesize if treatment with senolytics would have benefited those GB patients showing the crucial need for further research in this

field [64–66]. Treatment with IT might have also resulted in senescence re-induction, as observed in the analyzed R-clones, explaining the delay observed in patients 7 and 9, belonging to cluster 2. However, these patients exhibited no pronounced SASP. Thus, the recurrences of cluster 2 containing both IT-treated patients have possibly derived from cells which were able to avoid entering senescence in the first place. Interestingly enough, *CDKN1A* was upregulated in three out of four patients in this cluster. This suits well to results in LN428 cells, which express moderate but not inducible amounts of $p21^{CIP1}$ and were also resistant to senescence induction (Fig. S1A, Fig. S3).

In this study, we could show that IT is able to re-sensitize clones that escaped from TMZ-induced senescence in two ways: by upregulation of $p21^{CIP1}$ at protein level, and being capable of increasing senescence, but also cell death. Thus, we think that during the first weeks or couple of months after the first appearance of recurrence, IT could act in a similar way. The repercussions of this putative effect of IT therapy are visible in our transcription heatmap, showing what is 'left' in the final recurrence for surgery. Thus, in Rec7 (patient receiving IT), we observed repression of all genes investigated, apart from *EGR1*. Not only Rec7 but all recurrences in Cluster 2 exhibited repression of the DNA repair genes *MSH2*, *MSH6* and *EXO1* involved in mismatch repair, of apoptosis inhibitors (*BIRC2*, *BIRC5*, *XIAP*, *Bcl-xL*) and SASP factors (*CCL8, CXCL-1, IL-1α, IL-6*), which might implicate cell death. It is known that IT works more efficiently in the background of inactive MMR and dysfunctional or inhibited p53/ $p21^{CIP1}$pathway [41,67,68].

Overall, we showed that IT efficiently induced senescence in GB cells and that $p21^{CIP1}$, but not $p14^{ARF}$, $p16^{INK4A}$ or PTEN is decisively involved. Importantly, IT can also induce senescence and cell death in cell clones evading/escaping TMZ-induced senescence and these senescent cells can be targeted with the senolytic drug BV6. Learning from these encouraging results, it might be worthy of treating recurrent GB tumors with this combination.

Ethics approval

Ethics approval is a part of the Material Transfer Agreement with the French Glioblastoma Biobank (FGB, CHU Angers, BRIF n° BB-0033–00093) (April 25, 2022). All procedures were performed in compliance with relevant laws and institutional guidelines (Declaration of Helsinki) and have been approved by the ethics committee at the Rhineland-Palatinate State Medical Association (Application number 2022–16425, August 26, 2022).

Funding

This work was supported by the Wilhelm Sander Foundation [Project-ID 2019.154.1] to MTT and MCH; and the Deutsche Forschungsgemeinschaft (DFG, German Science Foundation) [Project-ID 508828494] to MTT.

CRediT authorship contribution statement

Markus Christmann: Validation, Investigation, Funding acquisition, Writing - review & editing. **Maja T Tomicic:** Writing – original draft, Visualization, Validation, Supervision, Investigation, Funding acquisition, Conceptualization, Writing - review & editing. **Jason Sallbach:** Visualization, Validation, Methodology, Investigation, Formal analysis, Data curation. **Melanie Woods:** Methodology, Investigation, Formal analysis. **Birgit Rasenberger:** Methodology, Investigation.

Declaration of Competing Interest

The authors declare that they have no known competing financial interests or personal relationships that could have appeared to influence the work reported in this paper.

Acknowledgments

We greatly acknowledge the French Glioblastoma Biobank (FGB, CHU Angers, BRIF n° BB-0033–00093) for providing biological material (shock-frozen tissue and FFPE microscope slides of primary and corresponding recurrent GB) and associated data. We thank Ariane Schmidt for helping us with supplementary tables containing PCR-primers and antibodies used in this study.

Consent to participate & consent for publication

Patients' consent to participate and patients' consent for publication of the data was provided by the French Glioblastoma Biobank (FGB, CHU Angers).

Appendix A. Supporting information

Supplementary data associated with this article can be found in the online version at doi:10.1016/j.biopha.2024.117634.

Data Availability

Data will be made available on request.

References

[1] D.N. Louis, A. Perry, P. Wesseling, D.J. Brat, I.A. Cree, D. Figarella-Branger, C. Hawkins, H. Ng, S.M. Pfister, G. Reifenberger, The 2021 WHO classification of tumors of the central nervous system: a summary, Neuro-Oncol. 23 (2021) 1231–1251.
[2] J.B. Vilar, M. Christmann, M.T. Tomicic, Alterations in molecular profiles affecting glioblastoma resistance to radiochemotherapy: where does the good go? Cancers (Basel) 14 (2022) https://doi.org/10.3390/cancers14102416.
[3] R. Stupp, W.P. Mason, M.J. van den Bent, M. Weller, B. Fisher, M.J. Taphoorn, K. Belanger, A.A. Brandes, C. Marosi, U. Bogdahn, et al., Radiotherapy plus concomitant and adjuvant temozolomide for glioblastoma, N. Engl. J. Med 352 (2005) 987–996.
[4] R. Stupp, M.E. Hegi, W.P. Mason, M.J. van den Bent, M.J. Taphoorn, R.C. Janzer, S. K. Ludwin, A. Allgeier, B. Fisher, K. Belanger, et al., Effects of radiotherapy with concomitant and adjuvant temozolomide versus radiotherapy alone on survival in glioblastoma in a randomised phase III study: 5-year analysis of the EORTC-NCIC trial, Lancet Oncol. (2009).
[5] B. Kaina, M. Christmann, DNA repair in resistance to alkylating anticancer drugs, Int J. Clin. Pharm. Ther. 40 (2002) 354–367.
[6] M.T. Tomicic, R. Meise, D. Aasland, N. Berte, R. Kitzinger, O.H. Krämer, B. Kaina, M. Christmann, Apoptosis induced by temozolomide and nimustine in glioblastoma cells is supported by JNK/c-Jun-mediated induction of the BH3-only protein BIM, Oncotarget 6 (2015) 33755.
[7] M. Christmann, K. Diesler, D. Majhen, C. Steigerwald, N. Berte, H. Freund, N. Stojanović, B. Kaina, M. Osmak, A. Ambriović-Ristov, Integrin αVβ3 silencing sensitizes malignant glioma cells to temozolomide by suppression of homologous recombination repair, Oncotarget 8 (2017) 27754.
[8] D. Aasland, L. Götzinger, L. Hauck, N. Berte, J. Meyer, M. Effenberger, S. Schneider, E.E. Reuber, W.P. Roos, M.T. Tomicic, Temozolomide induces senescence and repression of DNA repair pathways in glioblastoma cells via activation of ATR–CHK1, p21, and NF-κB, Cancer Res. 79 (2019) 99–113.
[9] T.R. Reich, C. Schwarzenbach, J.B. Vilar, S. Unger, F. Mühlhäusler, T. Nikolova, A. Poplawski, H. Baymaz, P. Beli, M. Christmann, Localization matters: Nuclear-trapped Survivin sensitizes glioblastoma cells to temozolomide by elevating cellular senescence and impairing homologous recombination, Cell. Mol. Life Sci. 78 (2021) 5587–5604.
[10] R. Chojak, J. Fares, E. Petrosyan, M.S. Lesniak, Cellular senescence in glioma, J. Neurooncol 164 (2023) 11–29, https://doi.org/10.1007/s11060-023-04387-3.
[11] L. Hayflick, The limited in vitro lifetime of human diploid cell strains, Exp. Cell Res 37 (1965) 614–636, https://doi.org/10.1016/0014-4827(65)90211-9.
[12] F. d'Adda di Fagagna, Living on a break: cellular senescence as a DNA-damage response, Nat. Rev. Cancer 8 (2008) 512–522, https://doi.org/10.1038/nrc2440.
[13] M.C. Velarde, M. Demaria, J. Campisi, Senescent cells and their secretory phenotype as targets for cancer therapy, Inter. Top. Gerontol. 38 (2013) 17–27, https://doi.org/10.1159/000343572.
[14] C.D. Wiley, M.C. Velarde, P. Lecot, S. Liu, E.A. Sarnoski, A. Freund, K. Shirakawa, H.W. Lim, S.S. Davis, A. Ramanathan, et al., Mitochondrial dysfunction induces senescence with a distinct secretory phenotype, Cell Metab. 23 (2016) 303–314, https://doi.org/10.1016/j.cmet.2015.11.011.
[15] J.-P. Coppé, P.-Y. Desprez, A. Krtolica, J. Campisi, The senescence-associated secretory phenotype: the dark side of tumor suppression, Annu. Rev. Pathol.: Mech. Dis. 5 (2010) 99–118.

[16] T. Kuilman, C. Michaloglou, L.C. Vredeveld, S. Douma, R. van Doorn, C.J. Desmet, L.A. Aarden, W.J. Mooi, D.S. Peeper, Oncogene-induced senescence relayed by an interleukin-dependent inflammatory network, Cell 133 (2008) 1019–1031, https://doi.org/10.1016/j.cell.2008.03.039.
[17] J.C. Acosta, A. O'Loghlen, A. Banito, M.V. Guijarro, A. Augert, S. Raguz, M. Fumagalli, M. Da Costa, C. Brown, N. Popov, et al., Chemokine signaling via the CXCR2 receptor reinforces senescence, Cell 133 (2008) 1006–1018, https://doi.org/10.1016/j.cell.2008.03.038.
[18] T.W. Kang, T. Yevsa, N. Woller, L. Hoenicke, T. Wuestefeld, D. Dauch, A. Hohmeyer, M. Gereke, R. Rudalska, A. Potapova, et al., Senescence surveillance of pre-malignant hepatocytes limits liver cancer development, Nature 479 (2011) 547–551, https://doi.org/10.1038/nature10599.
[19] W. Xue, L. Zender, C. Miething, R.A. Dickins, E. Hernando, V. Krizhanovsky, C. Cordon-Cardo, S.W. Lowe, Senescence and tumour clearance is triggered by p53 restoration in murine liver carcinomas, Nature 445 (2007) 656–660, https://doi.org/10.1038/nature05529.
[20] C. Bavik, I. Coleman, J.P. Dean, B. Knudsen, S. Plymate, P.S. Nelson, The gene expression program of prostate fibroblast senescence modulates neoplastic epithelial cell proliferation through paracrine mechanisms, Cancer Res 66 (2006) 794–802, https://doi.org/10.1158/0008-5472.CAN-05-1716.
[21] S. Parrinello, J.P. Coppe, A. Krtolica, J. Campisi, Stromal-epithelial interactions in aging and cancer: senescent fibroblasts alter epithelial cell differentiation, J. Cell Sci. 118 (2005) 485–496, https://doi.org/10.1242/jcs.01635.
[22] A. Krtolica, S. Parrinello, S. Lockett, P.Y. Desprez, J. Campisi, Senescent fibroblasts promote epithelial cell growth and tumorigenesis: a link between cancer and aging, Proc. Natl. Acad. Sci. USA 98 (2001) 12072–12077, https://doi.org/10.1073/pnas.211053698.
[23] R.M. Laberge, P. Awad, J. Campisi, P.Y. Desprez, Epithelial-mesenchymal transition induced by senescent fibroblasts, Cancer Micro 5 (2012) 39–44, https://doi.org/10.1007/s12307-011-0069-4.
[24] W. Wu, J.L. Klockow, M. Zhang, F. Lafortune, E. Chang, L. Jin, Y. Wu, H. E. Daldrup-Link, Glioblastoma multiforme (GBM): an overview of current therapies and mechanisms of resistance, Pharm. Res 171 (2021) 105780, https://doi.org/10.1016/j.phrs.2021.105780.
[25] H.S. Friedman, M.D. Prados, P.Y. Wen, T. Mikkelsen, D. Schiff, L.E. Abrey, W.K. A. Yung, N. Paleologos, M.K. Nicholas, R. Jensen, et al., Bevacizumab alone and in combination with irinotecan in recurrent glioblastoma, J. Clin. Oncol. 41 (2023) 4945–4952, https://doi.org/10.1200/JCO.22.02772.
[26] R. Ranchor, M.J.R.G.D.L. Ramos, R.M. Romao, A.S. Mendes, R.C. Pichel, J. Q. Coelho, E.M. Rosendo, M.J. Magalhaes, A.M.F. Araújo, 3P Bevacizumab plus irinotecan as second-line treatment of glioblastoma: Real-world evidence, ESMO Open 8 (2023) 101015, https://doi.org/10.1016/j.esmoop.2023.101015.
[27] Y. Pommier, Topoisomerase I inhibitors: camptothecins and beyond, Nat. Rev. Cancer 6 (2006) 789–802.
[28] D. Strumberg, A.A. Pilon, M. Smith, R. Hickey, L. Malkas, Y. Pommier, Conversion of topoisomerase I cleavage complexes on the leading strand of ribosomal DNA into 5′-phosphorylated DNA double-strand breaks by replication runoff, Mol. Cell Biol. 20 (2000) 3977–3987.
[29] Y. Wang, S. Zhu, T.F. Cloughesy, L.M. Liau, P.S. Mischel, p53 disruption profoundly alters the response of human glioblastoma cells to DNA topoisomerase I inhibition, Oncogene 23 (2004) 1283–1290.
[30] R.A. Weinberg, The retinoblastoma protein and cell cycle control, Cell 81 (1995) 323–330, https://doi.org/10.1016/0092-8674(95)90385-2.
[31] D.K. Dimova, N.J. Dyson, The E2F transcriptional network: old acquaintances with new faces, Oncogene 24 (2005) 2810–2826, https://doi.org/10.1038/sj.onc.1208612.
[32] D.A. Alcorta, Y. Xiong, D. Phelps, G. Hannon, D. Beach, J.C. Barrett, Involvement of the cyclin-dependent kinase inhibitor p16 (INK4a) in replicative senescence of normal human fibroblasts, Proc. Natl. Acad. Sci. USA 93 (1996) 13742–13747, https://doi.org/10.1073/pnas.93.24.13742.
[33] E. Hara, R. Smith, D. Parry, H. Tahara, S. Stone, G. Peters, Regulation of p16CDKN2 expression and its implications for cell immortalization and senescence, Mol. Cell Biol. 16 (1996) 859–867, https://doi.org/10.1128/MCB.16.3.859.
[34] G.H. Stein, L.F. Drullinger, A. Soulard, V. Dulic, Differential roles for cyclin-dependent kinase inhibitors p21 and p16 in the mechanisms of senescence and differentiation in human fibroblasts, Mol. Cell Biol. 19 (1999) 2109–2117, https://doi.org/10.1128/MCB.19.3.2109.
[35] J. Pomerantz, N. Schreiber-Agus, N.J. Liegeois, A. Silverman, L. Alland, L. Chin, J. Potes, K. Chen, I. Orlow, H.W. Lee, et al., The Ink4a tumor suppressor gene product, p19Arf, interacts with MDM2 and neutralizes MDM2's inhibition of p53, Cell 92 (1998) 713–723, https://doi.org/10.1016/s0092-8674(00)81400-2.
[36] Y. Zhang, Y. Xiong, W.G. Yarbrough, ARF promotes MDM2 degradation and stabilizes p53: ARF-INK4a locus deletion impairs both the Rb and p53 tumor suppression pathways, Cell 92 (1998) 725–734, https://doi.org/10.1016/s0092-8674(00)81401-4.
[37] F.J. Stott, S. Bates, M.C. James, B.B. McConnell, M. Starborg, S. Brookes, I. Palmero, K. Ryan, E. Hara, K.H. Vousden, et al., The alternative product from the human CDKN2A locus, p14(ARF), participates in a regulatory feedback loop with p53 and MDM2, EMBO J. 17 (1998) 5001–5014, https://doi.org/10.1093/emboj/17.17.5001.
[38] M.T. Tomicic, B. Kaina, Topoisomerase degradation, DSB repair, p53 and IAPs in cancer cell resistance to camptothecin-like topoisomerase I inhibitors, Biochim Biophys. Acta 1835 (2013) 11–27.
[39] R.H. Medema, R.E. Herrera, F. Lam, R.A. Weinberg, Growth suppression by p16ink4 requires functional retinoblastoma protein, Proc. Natl. Acad. Sci. USA 92 (1995) 6289–6293, https://doi.org/10.1073/pnas.92.14.6289.
[40] M. Christmann, C. Boisseau, R. Kitzinger, C. Berac, S. Allmann, T. Sommer, D. Aasland, B. Kaina, M.T. Tomicic, Adaptive upregulation of DNA repair genes following benzo(a)pyrene diol epoxide protects against cell death at the expense of mutations, Nucleic Acids Res 44 (2016) 10727–10743, https://doi.org/10.1093/nar/gkw873.
[41] M.T. Tomicic, C. Steigerwald, B. Rasenberger, A. Brozovic, M. Christmann, Functional mismatch repair and inactive p53 drive sensitization of colorectal cancer cells to irinotecan via the IAP antagonist BV6, Arch. Toxicol. 93 (2019) 2265–2277, https://doi.org/10.1007/s00204-019-02513-7.
[42] M.T. Tomicic, F. Kramer, A. Nguyen, C. Schwarzenbach, M. Christmann, Oxaliplatin-induced senescence in colorectal cancer cells depends on p14(ARF)-mediated sustained p53 activation. Cancers (Basel) 13 (2021) https://doi.org/10.3390/cancers13092019.
[43] A. Clavreul, G. Soulard, J.M. Lemee, M. Rigot, P. Fabbro-Peray, L. Bauchet, D. Figarella-Branger, P. Menei, network, F.G.B. the French glioblastoma biobank (FGB): a national clinicobiological database, J. Transl. Med 17 (2019) 133, https://doi.org/10.1186/s12967-019-1859-6.
[44] J.G. Herman, J.R. Graff, S. Myohanen, B.D. Nelkin, S.B. Baylin, Methylation-specific PCR: a novel PCR assay for methylation status of CpG islands, Proc. Natl. Acad. Sci. USA 93 (1996) 9821–9826.
[45] M. Esteller, S. Tortola, M. Toyota, G. Capella, M.A. Peinado, S.B. Baylin, J. G. Herman, Hypermethylation-associated inactivation of p14(ARF) is independent of p16(INK4a) methylation and p53 mutational status, Cancer Res 60 (2000) 129–133.
[46] C. Steigerwald, B. Rasenberger, M. Christmann, M.T. Tomicic, Sensitization of colorectal cancer cells to irinotecan by the Survivin inhibitor LLP3 depends on XAF1 proficiency in the context of mutated p53, Arch. Toxicol. 92 (2018) 2645–2648, https://doi.org/10.1007/s00204-018-2240-x.
[47] S.H. Jung, H.J. Hwang, D. Kang, H.A. Park, H.C. Lee, D. Jeong, K. Lee, H.J. Park, Y. G. Ko, J.S. Lee, mTOR kinase leads to PTEN-loss-induced cellular senescence by phosphorylating p53, Oncogene 38 (2019) 1639–1650, https://doi.org/10.1038/s41388-018-0521-8.
[48] M. Parisotto, E. Grelet, R. El Bizri, Y. Dai, J. Terzic, D. Eckert, L. Gargowitsch, J. M. Bornert, D. Metzger, PTEN deletion in luminal cells of mature prostate induces replication stress and senescence in vivo, J. Exp. Med 215 (2018) 1749–1763, https://doi.org/10.1084/jem.20171207.
[49] A. Sharma, A. Almasan, Autophagy and PTEN in DNA damage-induced senescence, Adv. Cancer Res 150 (2021) 249–284, https://doi.org/10.1016/bs.acr.2021.01.006.
[50] N. Ishii, D. Maier, A. Merlo, M. Tada, Y. Sawamura, A.C. Diserens, E.G. Van Meir, Frequent co-alterations of TP53, p16/CDKN2A, p14ARF, PTEN tumor suppressor genes in human glioma cell lines, Brain Pathol. 9 (1999) 469–479, https://doi.org/10.1111/j.1750-3639.1999.tb00536.x.
[51] J. Campisi, d'Adda di Fagagna, F. Cellular senescence: when bad things happen to good cells, Nat. Rev. Mol. Cell Biol. 8 (2007) 729–740, https://doi.org/10.1038/nrm2233.
[52] P.C. Wu, Q. Wang, L. Grobman, E. Chu, D.Y. Wu, Accelerated cellular senescence in solid tumor therapy, Exp. Oncol. 34 (2012) 298–305.
[53] M.V. Astle, K.M. Hannan, P.Y. Ng, R.S. Lee, A.J. George, A.K. Hsu, Y. Haupt, R. D. Hannan, R.B. Pearson, AKT induces senescence in human cells via mTORC1 and p53 in the absence of DNA damage: implications for targeting mTOR during malignancy, Oncogene 31 (2012) 1949–1962, https://doi.org/10.1038/onc.2011.394.
[54] M. Fischer, M. Quaas, A. Nickel, K. Engeland, Indirect p53-dependent transcriptional repression of Survivin, CDC25C, and PLK1 genes requires the cyclin-dependent kinase inhibitor p21/CDKN1A and CDE/CHR promoter sites binding the DREAM complex, Oncotarget 6 (2015) 41402–41417, https://doi.org/10.18632/oncotarget.6356.
[55] M. Fischer, M. Quaas, L. Steiner, K. Engeland, The p53-p21-DREAM-CDE/CHR pathway regulates G2/M cell cycle genes, Nucleic Acids Res 44 (2016) 164–174, https://doi.org/10.1093/nar/gkv927.
[56] Z. Song, Y. Pan, G. Ling, S. Wang, M. Huang, X. Jiang, Y. Ke, Escape of U251 glioma cells from temozolomide-induced senescence was modulated by CDK1/survivin signaling, Am. J. Transl. Res. 9 (2017) 2163–2180.
[57] C. Schwarzenbach, L. Tatsch, J.B. Vilar, B. Rasenberger, L. Beltzig, B. Kaina, M. T. Tomicic, M. Christmann, Targeting c-IAP1, c-IAP2, and Bcl-2 eliminates senescent glioblastoma cells following temozolomide treatment, Cancers 13 (2021) 3585.
[58] L. Beltzig, M. Christmann, B. Kaina, Abrogation of cellular senescence induced by temozolomide in glioblastoma cells: search for senolytics, Cells 11 (2022), https://doi.org/10.3390/cells11162588.
[59] Y. Tian, H. Li, T. Qiu, J. Dai, Y. Zhang, J. Chen, H. Cai, Loss of PTEN induces lung fibrosis via alveolar epithelial cell senescence depending on NF-kappaB activation. Aging Cell 18 (2019) e12858 https://doi.org/10.1111/acel.12858.
[60] C.M. Beausejour, A. Krtolica, F. Galimi, M. Narita, S.W. Lowe, P. Yaswen, J. Campisi, Reversal of human cellular senescence: roles of the p53 and p16 pathways, EMBO J. 22 (2003) 4212–4222, https://doi.org/10.1093/emboj/cdg417.
[61] J.P. Coppe, C.K. Patil, F. Rodier, Y. Sun, D.P. Munoz, J. Goldstein, P.S. Nelson, P. Y. Desprez, J. Campisi, Senescence-associated secretory phenotypes reveal cell-nonautonomous functions of oncogenic RAS and the p53 tumor suppressor, PLoS Biol. 6 (2008) 2853–2868, https://doi.org/10.1371/journal.pbio.0060301.
[62] T. Saleh, Therapy-induced senescence is finally escapable, what is next? Cell Cycle 23 (2024) 713–721, https://doi.org/10.1080/15384101.2024.2364579.

[63] T. Saleh, D.A. Gewirtz, Considering therapy-induced senescence as a mechanism of tumour dormancy contributing to disease recurrence, Br. J. Cancer 126 (2022) 1363–1365, https://doi.org/10.1038/s41416-022-01787-6.
[64] M.T. Tomicic, M. Christmann, Targeting anticancer drug-induced senescence in glioblastoma therapy, Oncotarget 9 (2018) 37466–37467, https://doi.org/10.18632/oncotarget.26502.
[65] J.L. Kirkland, T. Tchkonia, Senolytic drugs: from discovery to translation, J. Intern Med 288 (2020) 518–536, https://doi.org/10.1111/joim.13141.
[66] P.D. Robbins, D. Jurk, S. Khosla, J.L. Kirkland, N.K. LeBrasseur, J.D. Miller, J. F. Passos, R.J. Pignolo, T. Tchkonia, L.J. Niedernhofer, Senolytic drugs: reducing senescent cell viability to extend health span, Annu Rev. Pharm. Toxicol. 61 (2021) 779–803, https://doi.org/10.1146/annurev-pharmtox-050120-105018.
[67] M.T. Tomicic, M. Christmann, B. Kaina, Topotecan-triggered degradation of topoisomerase I is p53-dependent and impacts cell survival, Cancer Res 65 (2005) 8920–8926.
[68] M.T. Tomicic, M. Christmann, B. Kaina, Topotecan triggers apoptosis in p53-deficient cells by forcing degradation of XIAP and survivin thereby activating caspase-3-mediated Bid cleavage, J. Pharm. Exp. Ther. 332 (2010) 316–325.